

Simulating Subhalos at High Redshift: Merger Rates, Counts, and Types

Andrew R. Wetzel¹, J.D. Cohn², Martin White^{1,3}

¹*Department of Astronomy, University of California, Berkeley, CA 94720, USA*

²*Space Sciences Laboratory, University of California, Berkeley, CA 94720, USA*

³*Department of Physics, University of California, Berkeley, CA 94720, USA*

October 2008

ABSTRACT

Galaxies are believed to be in one-to-one correspondence with simulated dark matter subhalos. We use high-resolution N-body simulations of cosmological volumes to calculate the statistical properties of subhalo (galaxy) major mergers at high redshift ($z = 0.6 - 5$). We measure the evolution of the galaxy merger rate, finding that it is much shallower than the merger rate of dark matter host halos at $z > 2.5$, but roughly parallels that of halos at $z < 1.6$. We also track the detailed merger histories of individual galaxies and measure the likelihood of multiple mergers per halo or subhalo. We examine satellite merger statistics in detail: 15% – 35% of all recently merged galaxies are satellites and satellites are twice as likely as centrals to have had a recent major merger. Finally, we show how the differing evolution of the merger rates of halos and galaxies leads to the evolution of the average satellite occupation per halo, noting that for a fixed halo mass, the satellite halo occupation peaks at $z \sim 2.5$.

Key words: cosmology:theory – methods:N-body simulations – galaxies:halos – galaxies:interactions

1 INTRODUCTION

Mergers are key in the hierarchical growth of structure, and major galaxy mergers (referred to as mergers henceforth) are thought to play a crucial role in galaxy evolution. Specifically, they are expected to trigger quasar activity (e.g., Carlberg 1990), starbursts (e.g., Barnes & Hernquist 1991; Noguchi 1991), and morphological changes (e.g., Toomre & Toomre 1972), and they are thought to be related to Lyman Break Galaxies (LBGs), submillimeter galaxies (SMGs), and ultra-luminous infrared galaxies (ULIRGs) (see reviews by Giavalisco 2002; Blain et al. 2002; Sanders & Mirabel 1996, respectively). Observational samples of such objects at $z \gtrsim 1$ are now becoming large enough to allow for statistical analyses of their counts (e.g., Steidel et al. 2003; Ouchi et al. 2004; Coppin et al. 2006; Yoshida et al. 2006; Gawiser et al. 2007; Genel et al. 2008; McLure et al. 2008; Patton & Atfield 2008; Tacconi et al. 2008; Yamauchi et al. 2008).

Understanding galaxy mergers and their connection to these observables requires comparison with theoretical predictions. In simulations, galaxies are identified with subhalos, the substructures of dark matter halos (e.g. Ghigna et al. 1998; Moore et al. 1999; Klypin et al. 1999;

Ghigna et al. 2000).¹ Simulations are now becoming sufficiently high in resolution and large in volume to provide statistically significant samples (e.g. De Lucia et al. 2004; Diemand et al. 2004; Gao et al. 2004; Reed et al. 2005). This high mass and force resolution is necessary to track bound subhalos throughout their orbit in the host halo and avoid artificial numerical disruption. This is particularly important for tracking the orbits of galaxies, which are expected to reside in the dense inner core of subhalos and to be more stable to mass stripping than dark matter because of dissipative gas dynamics. The correspondence of galaxies with subhalos has been successful in reproducing galaxy counts and clustering in a wide array of measurements (e.g., Springel et al. 2001, 2005; Zentner et al. 2005; Bower et al. 2006; Conroy et al. 2006; Vale & Ostriker 2006; Wang et al. 2006). Henceforth, we will use the term galaxy and subhalo interchangeably.

A subhalo forms when two halos collide and a remnant of the smaller halo persists within the larger final halo. Thus, subhalo merger rates are sometimes inferred from halo merger rates² or subhalo distributions, using a dynamical

¹ A subhalo can comprise an entire halo if there are no other subhalos within the halo, see §2.

² Halo merger counts and rates have been studied in a vast literature, both estimated analytically (e.g., Kauffmann & White

friction model to estimate the infall time of satellite galaxies to their halo’s central galaxy (several of these methods are compared in Hopkins et al. 2008). However, a detailed understanding of galaxy mergers requires a sufficiently high-resolution simulation that can track the evolution and coalescence of subhalos directly.

Here we use high resolution dark matter simulations to examine subhalo merger rates, counts, and types, their mass and redshift dependence, and their relation to their host halos. Under the assumption that galaxies populate the centres of dark matter subhalo potential wells, our subhalos are expected to harbor massive galaxies ($L \gtrsim L_*$). Although our subhalo mass assignment is motivated by semi-analytic arguments, our results are independent of any specific semi-analytic modeling prescription.

Previous work on subhalo mergers includes both dark matter only simulations (Kolatt et al. 2000; Springel et al. 2001; De Lucia et al. 2004; Taylor & Babul 2005; Berrier et al. 2006; Wang & Kauffmann 2008; Mateus 2008) and hydrodynamic simulations (Murali et al. 2002; Tormen et al. 2004; Maller et al. 2006; Thacker et al. 2006; Simha et al. 2008). Many of these earlier studies concern subhalo mergers within a single object (such as the Milky Way or a galaxy cluster), others use lower resolution. We look at relatively large simulation volumes (100 and 250 h^{-1} Mpc boxes) with high spatial and temporal resolution. In addition, many previous works focus on subhalo mass loss and survival rate, while our main interest here is the population of resulting merged subhalos itself (most similar to the works of Maller et al. 2006; Guo & White 2008; Simha et al. 2008; Angulo et al. 2008). We characterize subhalo merger properties in detail, including satellite mergers, at high redshift ($z = 0.6 - 5$), during the peak of merger activity. We also investigate the satellite halo occupation (number of satellites per halo), and its evolution as shaped by the relative merger rates of subhalos and halos. The satellite halo occupation is a key element in the halo model (Seljak 2000; Peacock & Smith 2000; Berlind & Weinberg 2002; Cooray & Sheth 2002), a framework which describes large-scale structure in terms of host dark matter halos.

In §2 we describe the simulations, our definitions of halos and subhalos, their infall mass, and the evolution of the satellite fraction. In §3 we define our merger criteria and examine subhalo merger rates and their relation to halo merger rates. In §4 we explore the relative contributions of satellites and centrals to the merger population, both in terms of parents and merged children. §5 gives the distribution of the number of mergers within a given look-back time and the fraction of halos that host subhalo mergers. In §6 we show how the difference in halo and subhalo merger rates contributes to the evolution of the satellite halo occupation. We summarize and discuss in §7. The Appendices compare subhalo infall mass to infall maximum circular velocity and its evolution with redshift, and give our satellite subhalo

mass function. The halo occupation and clustering of high redshift galaxy mergers is treated in Wetzel et al. (2009).

2 NUMERICAL TECHNIQUES

2.1 Simulations

We use two dark matter only N-body simulations of 800^3 and 1024^3 particles in a periodic cube with side lengths $100h^{-1}$ Mpc and $250h^{-1}$ Mpc, respectively. For our Λ CDM cosmology ($\Omega_m = 0.25$, $\Omega_\Lambda = 0.75$, $h = 0.72$, $n = 0.97$ and $\sigma_8 = 0.8$), in agreement with a wide array of observations (Smoot et al. 1992; Tegmark et al. 2006; Reichardt et al. 2008; Komatsu et al. 2009), this results in particle masses of $1.4 \times 10^8 h^{-1} M_\odot$ ($1.1 \times 10^9 h^{-1} M_\odot$) and a Plummer equivalent smoothing of $4h^{-1}$ kpc ($9h^{-1}$ kpc) for the smaller (larger) simulation. The initial conditions were generated at $z = 200$ using the Zel’dovich approximation applied to a regular Cartesian grid of particles and then evolved using the *TreePM* code described in White (2002) (for a comparison with other codes see Heitmann et al. 2008; Evrard et al. 2008). Outputs were spaced every 50 Myr (~ 100 Myr) for the smaller (larger) simulation, from $z \sim 5$ to 2.5. Additional outputs from the smaller simulation were retained at lower redshift, spaced every ~ 200 Myr down to $z = 0.6$, below which we no longer fairly sample a cosmological volume. For mergers, we restrict these later outputs to $z < 1.6$ based on convergence tests of the merger rates (we lack sufficient output time resolution in the intervening redshifts to properly catch all mergers; see end of §3.1 for more). Our redshift range of $z = 0.6 - 5$ allows us to examine subhalos across 7 Gyr of evolution.

To find the subhalos from the phase space data we first generate a catalog of halos using the Friends-of-Friends (FoF) algorithm (Davis et al. 1985) with a linking length of $b = 0.168$ times the mean inter-particle spacing. This partitions the particles into equivalence classes by linking together all particles separated by less than b , with a density of roughly $\rho > 3/(2\pi b^3) \simeq 100$ times the background density. The longer linking length of $b = 0.2$ is often used. However, this linking length is more susceptible to joining together distinct, unbound structures and assigning a halo that transiently passes by another as a subhalo. Thus, we use a more conservative linking length, which for a given halo at our mass and redshift regime yields a $\sim 15\%$ lower mass than $b = 0.2$.³ We keep all FoF groups with more than 32 particles, and we refer to these groups as “(host) halos”. Halo masses quoted below are these FoF masses.

When two halos merge, the smaller halo can retain its identity as a “subhalo” inside the larger host halo. We identify subhalos (and sometimes subhalos within subhalos) using a new implementation of the *Subfind* algorithm

1993; Lacey & Cole 1993; Percival & Miller 1999; Benson et al. 2005; Zhang et al. 2008) and measured in simulations (e.g., Lacey & Cole 1994; Tormen 1998; Somerville et al. 2000; Cohn et al. 2001; Gottlöber et al. 2001; Cohn & White 2005; Li et al. 2007; Cohn & White 2008; Fakhouri & Ma 2008; Stewart et al. 2008).

³ Many Millennium subhalo studies use Spherical Overdensity (SO) halos based on an FoF(0.2) catalogue, in part to take out the extra structure joined by the larger linking length. Neto et al. (2007) compares the FoF(0.2) halo centres and those for the SO halos used to define the corresponding subhalo populations. More generally, White (2001) compares different mass definitions in detail, and Cohn & White (2008) discusses the relation of FoF(0.2), FoF(0.168), SO(180) and Sheth-Tormen (Sheth & Tormen 1999, based on $b = 0.2$) masses at high redshift.

(Springel et al. 2001). We take subhalos to be gravitationally self-bound aggregations of particles bounded by a density saddle point. After experimentation with different techniques we find this method gives a good match to what would be selected “by eye” as subhalos. We use a spline kernel with 16 neighbours to estimate the density and keep all subhalos with more than 20 particles. The subhalo that contains the most mass in the halo is defined as the central subhalo, all other subhalos in the same halo are satellites.⁴ The central subhalo is also assigned all matter within the halo not assigned to the satellite subhalos. The position of a subhalo is given by the location of its most bound particle, and the centre of a host halo is defined by the centre of its central subhalo. For each subhalo we store a number of additional properties including the bound mass, velocity dispersion, peak circular velocity, total potential energy, and velocity.

Figure 1 (top) shows the projected image of a sample halo of mass $2.2 \times 10^{12} h^{-1} M_{\odot}$, which hosts 12 satellite subhalos, at $z = 2.6$ in the $100 h^{-1}$ Mpc simulation. (At this redshift in our simulations there are approximately 200 halos per $(100 h^{-1} \text{ Mpc})^3$ above this mass.) Halos at this mass and redshift regime are dynamically active and often highly aspherical, with mean axial ratio (ratio of smallest-to-largest semi-major axes) of ~ 0.5 , and recently merged halos have even more discrepant axial ratios (Allgood et al. 2006). Figure 1 also shows how a halo’s densest region (figure centre), centre of mass, and substructure distribution can all be offset from one another. Because of these asymmetries, satellite subhalos sometimes extend well beyond r_{200c} , which we will call the halo virial radius.⁵

2.2 Subhalo Tracking

We identify, for each subhalo, a unique “child” at a later time, using subhalo tracking similar to Springel et al. (2005), Faltenbacher et al. (2005), Allgood (2005) and Harker et al. (2006). We detail our method to illustrate the subtleties which arise and to allow comparison with other work.

We track histories over four consecutive simulation outputs at a time because nearby subhalos can be difficult to distinguish and can “disappear” for a few outputs until their orbits separate them again. For each subhalo with mass M_1 at scale factor a_1 , its child subhalo at a later time (scale factor a_2 and mass M_2) is that which maximizes

$$\alpha = f(M_1, M_2) \ln^{-1} \left(\frac{a_2}{a_1} \right) \sum_{i \in 2} \phi_{1i}^2 \quad (1)$$

where

$$f(M_1, M_2) = \begin{cases} 1 - \frac{|M_1 - M_2|}{M_1 + M_2} & M_1 < M_2 \\ 1 & M_1 \geq M_2 \end{cases} \quad (2)$$

⁴ In most cases, the central subhalo in *Subfind* is built around the most bound and most dense particle in the group. However, this is not always the case.

⁵ The halo virial radius, r_{200c} , i.e. the radius within which the average density is $200 \times$ the critical density, is calculated from the FoF ($b = 0.168$) mass by first converting to M_{200c} assuming a spherical NFW (Navarro et al. 1996) density profile, and then taking $M_{200c} = 200 \frac{4\pi}{3} \rho_c r_{200c}^3$.

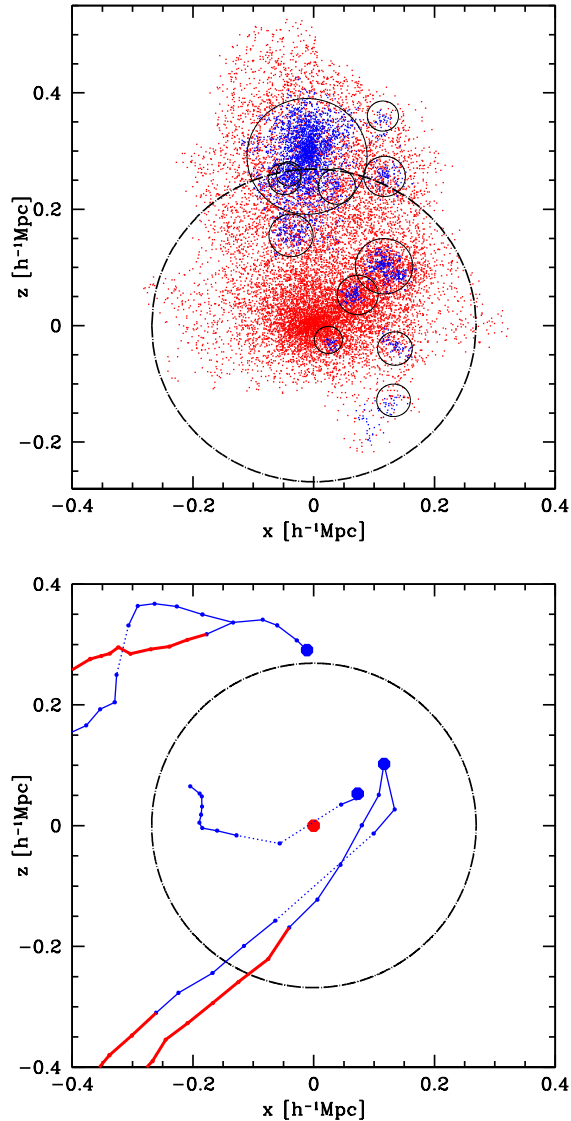


Figure 1. Top: Projected image of a halo of mass $2.2 \times 10^{12} h^{-1} M_{\odot}$ at $z = 2.6$ which hosts 12 satellite subhalos. Particles assigned to the central subhalo are red, while those assigned to satellite subhalos are blue. Dot-dashed circle shows the halo’s virial radius (r_{200c}), derived from its mass assuming a spherical NFW density profile, while the solid circles highlight the satellite subhalos and scale in radius with their mass. The central subhalo has bound mass of $1.8 \times 10^{12} h^{-1} M_{\odot}$, so nearly 20% of the halo’s mass lies in satellite subhalos. **Bottom:** Tracking histories of massive satellite subhalos in the above halo. Large dots show the positions of satellite subhalo centres at $z = 2.6$ for subhalos that had a mass $> 10^{11} h^{-1} M_{\odot}$ when they fell into the halo. Small dots show their positions (relative to that of the halo centre) at each output (spaced 50 Myr) back 800 Myr. Thin blue curves show subhalo trajectories when they are satellites while thick red curves show when they are centrals (before falling into the halo). Dotted lines indicate when the parent-child assignment has skipped an output (during a fly-by near another subhalo).

and where ϕ_{1i} is the potential of particle i computed using all of the particles in subhalo 1, and the sum is over those of the 20 most bound particles in the progenitor that also lie in the candidate child. We track using only the 20 most bound particles since our ultimate interest is in galaxies, which we expect to reside in the highly bound, central region of the subhalo (20 is the minimum particle count for our subhalos). We do not use all the progenitor particles because summing over all of the particles in the progenitor that also lie in the child candidate leads to instances of parent-child assignment in which the child subhalo does not contain the most bound particles of its parent. Finally, we weight against large mass gains with a mass weighting factor so that smaller subhalos passing through larger ones and emerging later on the other side are correctly assigned as fly-by's and not mergers. We find $\sim 95\%$ of subhalos have a child in the next time step, with $\sim 4\%$ percent skipping one or more output times and $\sim 1\%$ having no identifiable child.

Figure 1 (bottom) shows the tracking histories of the most massive subhalos within the halo shown in Fig. 1 (top), for subhalos that had a mass $> 10^{11} h^{-1} M_{\odot}$ when they fell into the halo. The upper-most subhalo was a separate halo ($M = 1.3 \times 10^{12} h^{-1} M_{\odot}$) hosting its own massive satellite subhalo. It then fell into the main halo and then both (now satellite) subhalos merged with each other. The right-most subhalo is an example of two separate halos falling into the main halo, becoming satellites, and subsequently merging with each other. Finally, the track through the centre shows a single subhalo falling towards the central subhalo. Instead of merging with the central, it passes through as a fly-by.

All of these tracks show instances where the parent-child assignment algorithm has skipped an output (dotted lines) as one subhalo passes through another and re-emerges on the other side. Note also that, while the dot-dashed circle shows the halo virial radius, r_{200c} (at the last output), based on its mass assuming a spherical NFW density profile, the locations of the transitions of central subhalos to satellites during infall show that the spherical virial radius is only a rough approximation.

As a halo falls into a larger host halo and becomes a satellite subhalo, mass loss from tidal stripping can be extreme (90% or more) as the satellite subhalo orbits towards the centre of its host halo. Figure 2 shows the evolution from infall of a long-lived satellite with infall mass $M_{\text{inf}} = 6 \times 10^{11} h^{-1} M_{\odot}$ and maximum circular velocity at infall of $V_{c,\text{inf}} = 258 \text{ km/s}$. Mass and maximum circular velocity ($V_{c,\text{max}}^3$) are stripped by $\sim 90\%$ by the time the satellite first reaches pericentre. After pericentric passage, a satellite can also gain mass and circular velocity as it moves away from the dense centre of its host halo. This is shown in Fig. 2 where mass and circular velocity strongly correlate with radial distance throughout the orbit. This is partially an effect of our subhalo finder: the density contrast of a subhalo, which defines its physical extent and hence its mass, drops as it moves to a region of higher background density.⁶ However, this is also driven by a physical effect: as a satellite approaches the dense centre of its host halo, it will be compressed by tidal shocks in response to the

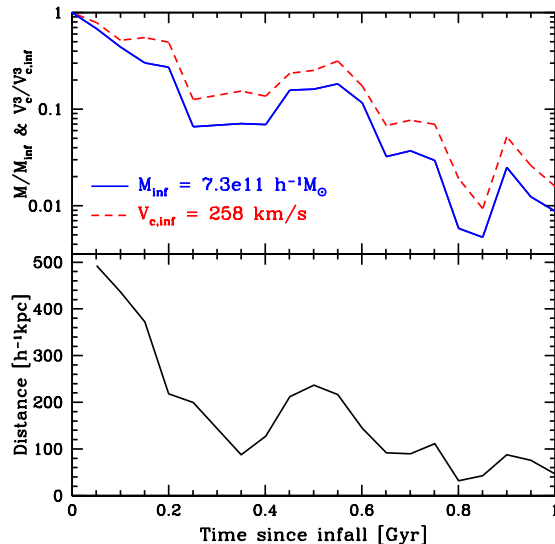


Figure 2. **Top:** Evolution of mass (solid curve) and circular velocity (dashed curve) as a function of time since infall for a satellite that fell into a halo of mass $8 \times 10^{12} h^{-1} M_{\odot}$ at $z = 3.7$. **Bottom:** Radial distance of satellite from centre of host halo. Mass and circular velocity exhibit correlations with radial distance, such as mass gain as the satellite recedes from the centre of its host halo. This satellite experienced no major merger activity throughout its history.

rapidly increasing potential (see Fig. 12 of Diemand et al. 2007; Gnedin & Ostriker 1997; Dekel et al. 2003).

Since a central subhalo is defined as the most massive subhalo, a satellite subhalo can become a central (and vice versa), which we refer to as a “switch”.⁷ We find that $\sim 4\%$ of all centrals at any output become satellites within the same halo in the next output, and of these a third immediately return to being centrals in the following output. Switches are twice as common during a merger event, either when two satellites merge, or when a satellite merges with the central, forming a less dense object and allowing another satellite to bind more mass to itself. When a satellite switches to a central and back to a satellite, the original satellite can be mistakenly assigned as a direct parent of the final satellite (and thus the central is assigned no parent) since our child assignment weights against large mass gains (which occurs when a satellite becomes a central). We fix these distinct cases by hand.

These switches highlight the fact that the distinction between a central and satellite subhalo is often not clear-cut: at this redshift and mass regime massive halos undergo rapid merger activity and thus often are highly disturbed and aspherical, with no well-defined single peak that represents the center of the halo profile.

⁶ A fly-by, i.e. when a subhalo passes through and is temporarily indistinguishable from a larger subhalo, is an extreme case of this.

⁷ In more detail, a switch occurs when the density peak of a satellite (above the background) contains more mass than is within the central subhalo’s radius at the position of the satellite

2.3 Subhalo Mass Assignment

Since we use subhalos as proxies for galaxies, we track subhalo mass that is expected to correlate with galaxy stellar mass. Galaxies form at halo centres as baryons cool and adiabatically contract toward the minimum of the halo’s potential well, which leads to a correlation between halo mass and galaxy stellar mass (White & Rees 1978; Blumenthal et al. 1986; Dubinski 1994; Mo et al. 1998). When a halo falls into a larger halo and becomes a satellite subhalo, its outskirts are severely stripped as discussed above, but its galaxy’s stellar mass would be little influenced as the galactic radius is typically $\sim 10\%$ that of the subhalo radius. This motivates assigning to subhalos their mass at infall, M_{inf} , which is expected to correlate with galactic stellar mass throughout the subhalo’s lifetime. The subhalo infall mass function has been successful at reproducing the observed galaxy luminosity function and clustering at low redshifts (Vale & Ostriker 2006; Wang et al. 2006; Yang et al. 2009). Maximum circular velocity at infall, $V_{\text{c,inf}}$, has also been successfully matched to some observations (Conroy et al. 2006; Berrier et al. 2006). In Appendix A we show the relation between M_{inf} and $V_{\text{c,inf}}$ and its redshift evolution.

Our prescription for assigning M_{inf} to subhalos is as follows. When a halo falls into another and its central subhalo becomes a satellite subhalo, the satellite is assigned M_{inf} as the subhalo mass of its (central) parent.⁸ If a satellite merges with another satellite, the resultant child subhalo is assigned the sum of its parents’ M_{inf} . Since the central subhalo contains the densest region of a halo, inter-halo gas is expected to accrete onto it, so we define M_{inf} for a central subhalo as its current self-bound subhalo mass, which is typically $\sim 90\%$ of its host halo’s mass.⁹ However, since a central subhalo can switch to being a satellite, while a satellite switches to being a central (all within a single host halo), we require an additional rule because using the above simple assignment of M_{inf} to centrals would lead to a central and satellite in a halo each having the halo’s current bound mass. Thus, we assign a central to have M_{inf} as its current self-bound subhalo mass only if it was the central in the same halo in the previous output. Thus, if a satellite switches to a central and remains the central for multiple outputs, it has robustly established itself as the central subhalo, so it is assigned its current self-bound mass. However, if a central was a satellite (or a central in another smaller halo) in the previous output, it is assigned the sum of its parents’ M_{inf} , with the additional requirement that its M_{inf} cannot exceed its current self-bound mass.

A small fraction ($\sim 4\%$) of satellites composed of at least 50 particles are not easily identifiable with any progenitor subhalos and thus cannot be tracked to infall. On inspection, we find that these “orphaned” satellites are loosely self-

bound portions of a central subhalo, remnants from a collision between a satellite and its central subhalo that soon re-merge with the central. Given their origins and fates, these orphans are not expected to host galaxies and are ignored.

Although we track subhalos down to 20 particles, we impose a much larger minimum infall mass to our sample to avoid selecting subhalos that artificially dissolve and merge with the central too early. This requires sufficient resolution of the radial density profile of a satellite subhalo at infall: if the satellite’s core is smaller than a few times the force softening length, its profile will be artificially shallow and it will be stripped and disrupted prematurely (see Appendices for details). For calibration, we use the regime of overlap in mass between our two simulations of different mass resolution, requiring consistent subhalo mass functions, halo occupation distributions, and merger statistics for a minimum infall mass. For example, going too low in mass for the larger simulation resulted in more mergers and fewer satellites than for the same mass range in the smaller simulation. In the larger simulation, our consistency requirements led us to impose $M_{\text{inf}} > 10^{12} h^{-1} M_{\odot}$. For a fixed number of particles per subhalo, this scales down to $M_{\text{inf}} > 10^{11} h^{-1} M_{\odot}$ in the smaller, higher resolution simulation. Note that halos of mass 10^{11} (10^{12}) $h^{-1} M_{\odot}$ cross below M_* , the characteristic mass of collapse, at $z = 1.5$ ($z = 0.8$), so we probe massive subhalos across most of our redshift range.

At $z = 2.6$, there are ~ 16000 subhalos with $M_{\text{inf}} > 10^{11} h^{-1} M_{\odot}$ in our $100 h^{-1}$ Mpc simulation and 9400 subhalos with $M_{\text{inf}} > 10^{12} h^{-1} M_{\odot}$ in our $250 h^{-1}$ Mpc simulation. At $z = 1$, there are ~ 29400 (2500) subhalos with $M_{\text{inf}} > 10^{11}$ (10^{12}) $h^{-1} M_{\odot}$ in our $100 h^{-1}$ Mpc simulation.

2.4 A Note on Stellar Mass and Gas Content of Subhalo Galaxies

A galaxy’s stellar mass is expected to be a non-linear, redshift-dependent function of its subhalo mass. An approximate relation based on abundance matching is given in Conroy & Wechsler (2008). At $z = 1$, they find that subhalos of infall mass 10^{11} (10^{12}) $h^{-1} M_{\odot}$ host galaxies of stellar mass $\sim 10^9$ ($10^{10.5}$) M_{\odot} . At $z = 2.5$, subhalos at the above masses are expected to host lower mass galaxies, though quantitative relations at this redshift are less certain, and our subhalo and halo finders differ in detail from theirs. Our sample of $M_{\text{inf}} > 10^{12} h^{-1} M_{\odot}$ subhalos approximately corresponds to $L \gtrsim L_*$ galaxies at the redshifts we examine.

Although our simulations do not track the baryonic content of subhalos, most massive galaxies are gas-rich at high redshift. That is, at $z \approx 1$, 70% to 90% of $L \sim L_*$ galaxies are observed to be blue (Cooper et al. 2007; Gerke et al. 2007), possessing enough gas to be actively star forming. The fraction of gas-rich galaxies at higher redshift is more poorly constrained but is thought to be higher (Hopkins et al. 2008). Thus, we anticipate that most, if not all, mergers we track have the capacity to drive galaxy activity such as starbursts and quasars.

2.5 Satellite Fraction

To frame our ensuing discussion of mergers, and the relative importance of satellite and central subhalos, Fig. 3 shows

⁸ There is some dependence on output time spacing in this definition: since a central subhalo typically continues to gain mass before it falls into a larger halo, shorter time steps (which catch it closer to infall) lead to a higher subsequent satellite M_{inf} . Doubling the output spacing leads to satellites with $\sim 10\%$ lower infall mass.

⁹ Though because of finite resolution, we find a weak systematic drop in $M_{\text{cen}}/M_{\text{halo}}$ with halo mass, varying from 93% to 87% for 10^{11} to $10^{14} h^{-1} M_{\odot}$ in the higher resolution simulation.

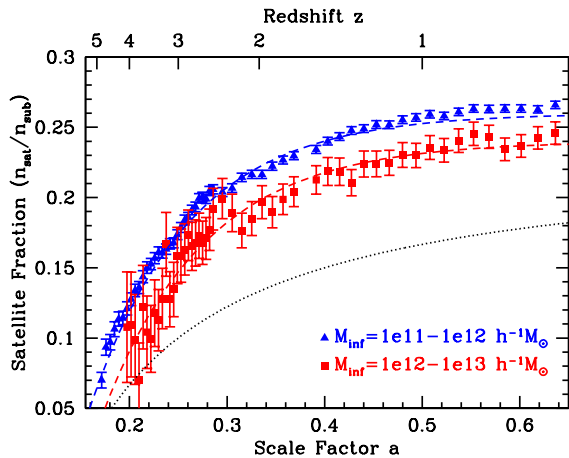


Figure 3. Evolution of the fraction of all subhalos that are satellites for $M_{\text{inf}} = 10^{11} - 10^{12} h^{-1} M_{\odot}$ (triangles) and $M_{\text{inf}} = 10^{12} - 10^{13} h^{-1} M_{\odot}$ (squares). Dashed lines show fits to Eq. 3. Dotted line shows fit to Eq. 4 (that of Conroy & Wechsler (2008)).

the evolution of the satellite fraction, $n_{\text{satellite}}/n_{\text{subhalo}}$, for subhalos of a fixed mass¹⁰, which grows monotonically with time from $z = 5 - 0.6$, as

$$\frac{n_{\text{satellite}}}{n_{\text{subhalo}}} = C - e^{-\frac{\beta}{1+z}} \quad (3)$$

with $\beta = 9.7$ valid across all subhalo masses and $C = 0.26$ (0.24) for lower (higher) mass. The satellite fraction decreases with increasing subhalo mass since more massive subhalos are more likely to be centrals, and for a fixed subhalo mass the satellite fraction increases with time as the number of high mass halos hosting massive satellites increases. The increase in the satellite fraction is slowed at late times because the number of massive satellites in halos of a fixed mass decreases with time as the satellites coalesce with the central subhalo (see §6).

Note that Eq. 3 predicts a much higher satellite fraction than that of Conroy & Wechsler (2008), who found

$$\frac{n_{\text{satellite}}}{n_{\text{subhalo}}} = 0.2 - \frac{0.1}{3}z. \quad (4)$$

It is unlikely that the difference is driven by numerical effects, since both their and our simulations are of similar mass resolution and volume, and both analyses are based on similar subhalo infall mass cuts (we see similar satellite fractions selecting instead on fixed $V_{c,\text{infall}}$). One likely factor is that, as noted above, our smaller output spacing yields higher infall mass for satellite subhalos, since we catch halos closer to infall when their mass is higher. In addition, they use a different halo and subhalo finding algorithm (Klypin et al. 1999; Kravtsov et al. 2004), and their higher σ_8 (0.9 rather than our 0.8) would give a lower merger rate and thus fewer satellites (one expects satellite survival timescales not to change). If normalized to the same satellite fraction at a given epoch, the redshift evolution of Eqs. 3 and 4 are in rough agreement.

¹⁰ We show the satellite fraction for two mass bins, but since the mass function falls exponentially at these masses and redshifts, almost all objects are at the low end of the mass bin. Using instead a minimum mass cut changes our results by only a few percent.

3 MERGER CRITERIA AND RATES

3.1 Merger Criteria

For two parents with $M_{\text{inf},2} \leq M_{\text{inf},1}$ sharing the same child subhalo at the next output they appear, a child is flagged as a (major) merger if $\frac{M_{\text{inf},2}}{M_{\text{inf},1}} > \frac{1}{3}$. If a child has more than two parents, we count multiple mergers if any other parents also exceed the above mass ratio with respect to the most massive parent.

Our mass ratio represents a trade-off between strong mergers (to maximize signal) and frequent merging (for statistical power). Galaxy mergers with stellar mass ratios closer than 3:1 are expected to drive interesting activity, e.g. quasars and starbursts, as mentioned above.¹¹

For generality, the distribution of merger (infall) mass ratios, $R:1$, for both halos and subhalos in the mass and redshift regimes we consider can be approximated by

$$f(R) \propto R^{-1.1} \quad (5)$$

in reasonable agreement with the $R^{-1.2}$ distribution of galaxy mass ratios at $z < 0.5$ found in hydrodynamic simulations by Maller et al. (2006).¹² Thus, the counts/rates of mergers with (infall) mass ratio closer than $R:1$ can be approximately scaled from our results through the relation

$$N(< R) = 8.6 (R^{0.1} - 1) N(< 3). \quad (6)$$

Sometimes merger criteria are based on instantaneous subhalo mass gain Thacker et al. (e.g., 2006). However, as exemplified in Fig. 2, subhalos can gain significant mass without coalescence. We find that most cases of significant subhalo mass gain are not a two-body coalescence, and so we do not use this to select mergers (see Wetzel et al. (2009) for more detail, also related results in Maulbetsch et al. (2007)).

Sufficient output time resolution is necessary to properly resolve the merger population. Unless otherwise stated, we use the shortest simulation output spacing to define the subhalo merger time interval, corresponding to 50 Myr (~ 100 Myr) for $M_{\text{inf}} > 10^{11}$ (10^{12}) $h^{-1} M_{\odot}$ at $z > 2.5$, and ~ 200 Myr for all masses at $z < 1.6$. By tracking parent/child subhalo assignments across multiple output spacings, we found that longer output time spacings result in a lower subhalo merger rate, arising from a combination of effects. As stated above, shorter time steps catch halos closer to their infall, resulting in satellites with higher M_{inf} , and hence more major satellite-central mergers. In addition, satellite-satellite mergers can be missed if their child merges into the central subhalo before the next time step. However, smaller output spacings are also more susceptible to switches, which can yield satellites with higher mass.

For halos, very short time steps can artificially enhance the merger rate, catching transient behavior as halos intersect, pass through each other, and re-merge. While we use

¹¹ Since galaxy stellar mass is a non-linear function of subhalo mass, a subhalo mass ratio of 3:1 may correspond to a galaxy merger of a more or less discrepant mass ratio. However, since the $M_{\text{stellar}} - M_{\text{subhalo}}$ relation is expected to peak for $M_{\text{subhalo}} \sim 10^{12} h^{-1} M_{\odot}$ (Conroy & Wechsler 2008), we do not expect this effect to strongly bias our results.

¹² The distribution of merger mass ratios also agrees well with the fit for halos at $z = 0$ provided by Wetzel et al. (2008).

FoF(0.168) instead of FoF(0.2) halos to help minimize artificial bridging effects, for a 50 Myr time spacing halo re-mergers still constitute a significant fraction of halo mergers. Thus we calculate all our halo mergers using > 100 Myr output spacings, for which halo re-mergers constitute only a few percent of all mergers.

Given our simulation volumes we are unable to probe statistically significant subhalo merger counts in halos more massive than $4 \times 10^{13} h^{-1} M_{\odot}$ at $z > 2.5$ and $M \sim 10^{14} h^{-1} M_{\odot}$ at $z < 1.6$. However, the majority of recently merged subhalos are centrals (discussed below), and selecting on higher mass host halos for a fixed subhalo mass restricts increasingly to recently merged satellites (of which there are comparatively fewer). Furthermore, nearly all subhalo mergers at a given mass occur in halos at most $5 - 10 \times$ times more massive.

3.2 Fits to Simulation

Figure 4 shows the evolution of the merger rate per object—defined as the number of mergers per time per object—for both subhalos and halos of the same (infall) mass.¹³ We fit the merger rate per object as

$$\frac{n_{\text{merge}}}{n_{\text{obj}} dt} = A(1+z)^{\alpha} \quad (7)$$

where n_{merge} is the number of (sub)halos whose parents match our mass ratio selection, n_{obj} is the total number of (sub)halos within the same mass range at the same output, and dt is the time interval between consecutive outputs. The best-fit values in each redshift regime are shown in Table 1. Note that the merger rate we examine is the number of mergers per time *per object*, different from another common definition, the number of mergers per time *per volume*.¹⁴

The relation of subhalo mergers to halo mergers is non-trivial. Although subhalo mergers are the eventual result of halo mergers, the former are governed by dynamics within a halo and the latter by large-scale gravitational fields. For halos, both the slope and the amplitude of the merger rate exhibit little dependence on mass or redshift. Similarly, e.g. Fakhouri & Ma (2008) found $\alpha = 2 - 2.3$ for all halo masses at $z < 6$, and weak halo mass dependence of the amplitude. In contrast, the subhalo merger rate amplitude has strong dependence on mass and its slope depends strongly on redshift. Relative to the halo merger rate, the subhalo merger rate is lower in amplitude than that of halos of the same (infall) mass, and, most notably at $z > 2.5$, the rate of subhalo mergers falls off significantly more slowly than that of halos. This is consistent with earlier work: De Lucia et al. (2004)

¹³ Merger fraction errors are calculated using binomial statistics. Given M mergers out of N objects, the most likely fraction is $f = M/N$ with variance $\sigma_f^2 = \frac{M(N-M)+1+N}{(N+2)^2(N+3)}$.

¹⁴ The former is simply the latter divided by the number density of objects of the same mass, but the merger rate per volume has qualitatively different behaviour because the (comoving) number density of objects at a fixed mass increases with time in a redshift-dependent manner. Specifically, at high redshift where the mass function rapidly increases, the merger rate per volume for both halos and subhalos *increases* with time, reaching a peak at $z \sim 2.5$. Below this redshift, it decreases with time in a power law manner as in Fig. 4, though with a shallower slope of $\alpha \approx 1.5$.

found a higher merger fraction for halos than subhalos, and Guo & White (2008) found strong mass dependence of the galaxy merger rate amplitude and that the slope becomes much shallower at $z > 2$ (see also Mateus 2008). (Note that as our halos are FoF(0.168) halos and so our merger rates can differ from those for FoF(0.2) halos; merging occurs sooner for a finder with a larger linking length.)

We now focus on the relation between halo and subhalo merger rates to understand these trends with time.

3.3 Subhalo vs. Halo Merger Rates

A simple analytic argument based on dynamical infall time, i.e., subhalo mergers are simply a delayed version halo mergers, leads one to expect that subhalo merger rates simply track those of halos: they have the same time evolution, with the subhalo merger rate having a higher amplitude. In this argument, when two halos merge, the new satellite galaxy collides with the other central galaxy within a dynamical friction timescale, approximated by

$$t_{\text{merge}} \approx C_o \frac{M_{\text{halo}}/M_{\text{sat}}}{\ln(1 + M_{\text{halo}}/M_{\text{sat}})} t_{\text{dyn}} \quad (8)$$

where $t_{\text{dyn}} = 0.1 t_{\text{Hubble}}$, $t_{\text{Hubble}} = \frac{1}{H(z)}$, and $C_o \approx 1$ accounts for the ensemble averaged satellite orbital parameters (Conroy et al. 2007; Binney & Tremaine 2008; Boylan-Kolchin et al. 2008; Jiang et al. 2008). Thus, for a fixed mass ratio, letting $m_o = M_{\text{halo}}/M_{\text{sat}}/\ln(1 + M_{\text{halo}}/M_{\text{sat}})$,

$$t_{\text{sat,merge}} \approx 0.1 C_o m_o t_{\text{Hubble}} \approx 0.1 C_o m_o t. \quad (9)$$

The evolution of the halo merger rate per object during matter-domination (valid at the high redshifts we examine), where $a \propto t^{2/3}$, is approximately

$$\frac{n_{\text{merge}}}{n_{\text{halo}} dt} = A(1+z)^{\alpha} = \left(\frac{t}{t_*}\right)^{-\frac{2}{3}\alpha}, \quad (10)$$

with t_* some proportionality constant. Assuming all halo mergers lead to satellite-central subhalo mergers on a dynamical friction timescale, the subhalo merger rate per object would evolve with time as

$$\frac{n_{\text{merge}}}{n_{\text{subhalo}} dt} = \left(\frac{t - t_{\text{sat,merge}}}{t_*}\right)^{-\frac{2}{3}\alpha} \quad (11)$$

$$= (1 - 0.1 C_o m_o)^{-\frac{2}{3}\alpha} \left(\frac{t}{t_*}\right)^{-\frac{2}{3}\alpha} \quad (12)$$

and so the subhalo merger rate would simply track that of halos of the same mass, but with higher amplitude.

3.4 Resolving the Discrepancy

As Fig. 4 shows, however, this tracking does not occur, particularly at high redshift where the slope of the subhalo merger rates is much shallower than that of halos. One reason for this is that we compute the merger rate per object, in which we divide by the number of objects at the given mass, $n_{\text{obj}}(m)$. Since halo masses are added instantaneously during halo mergers, a recently merged halo will instantly jump to a higher mass regime (with smaller n_{obj} in Eq. 7). In contrast, the central subhalo of the resultant halo will remain at a smaller mass for some time until its mass grows

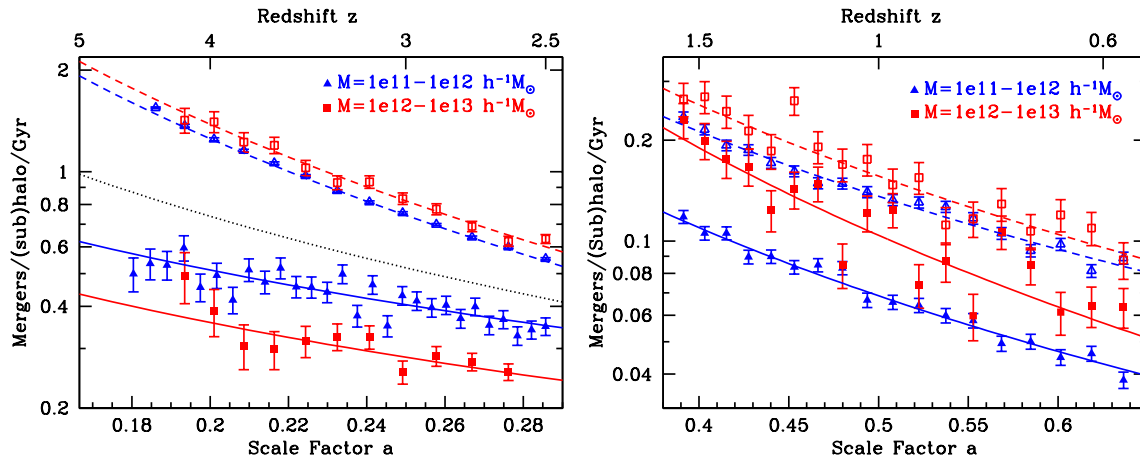


Figure 4. **Left:** Merger rate per object of subhalos (solid points) and halos (open points) as a function of the scale factor, for $M_{\text{inf}} = 10^{11} - 10^{12} h^{-1} M_{\odot}$ (triangles) and $M_{\text{inf}} = 10^{12} - 10^{13} h^{-1} M_{\odot}$ (squares) at $z = 5 - 2.5$. Solid (dashed) curves show fits of subhalo (halo) merger rates to Eq. 7, with fit parameters given in Table 1. **Right:** Same, but at $z = 1.6 - 0.6$. Also shown at left is the fit to the halo merger rate for halos with a central subhalo of $M_{\text{inf}} = 10^{11} - 10^{12} h^{-1} M_{\odot}$ (dotted).

Redshift		$z = 5 - 2.5$		$z = 1.6 - 0.6$	
Mass [$h^{-1} M_{\odot}$]		$10^{11} - 10^{12}$	$10^{12} - 10^{13}$	$10^{11} - 10^{12}$	$10^{12} - 10^{13}$
Halos	A	0.029	0.032	0.034	0.034
	α	2.3	2.3	2.0	2.2
Subhalos	A	0.093	0.065	0.016	0.016
	α	1.1	1.1	2.1	2.6

Table 1. The amplitude, A , and power law index, α , for halo and subhalo merger rates fit to Eq. 7.

from stripping of the new satellite subhalo (i.e., recently merged halos have lower than average $M_{\text{inf, cen}}/M_{\text{halo}}$), so the central's n_{obj} is higher.

In Fig. 4 (left) the dotted black curve fits the halo merger rate for halos selected with the same mass cut on their central subhalo infall mass. The amplitude is significantly smaller, and the slope is also shallower ($\alpha = 1.6$) than for halos selected on full halo mass, showing that the above effect is stronger at earlier times. By the argument above, the ratio of amplitudes of the merger rate per object of halos to subhalos is $n_{\text{halo}}/n_{\text{cen}}$. A fixed (sub)halo mass cut probes lower $M/M_*(t)$ at later times, and the mass function drops exponentially with increasing $M/M_*(t)$ at these masses. Thus, a fixed $M_{\text{inf, cen}}/M_{\text{halo}}$ after a halo merger means $n_{\text{halo}}/n_{\text{cen}}$ becomes closer to unity at later times, leading to the shallower slope.

The measured subhalo mergers have an even lower amplitude and shallower slope than the dotted line in Fig. 4, driven by two additional effects. First, a halo major merger might not lead to a subhalo major merger since the satellite-central merger mass ratio can be smaller than the mass ratios of their source halos. This is because M_{inf} naturally grows for a central but only grows for a satellite if it has a merger before coalescing with the central (see Wang & Kauffmann 2008, for a detailed analysis of this effect in terms of assigning baryons to subhalos). Since halos grow in mass more quickly at higher redshift, this effect is stronger at earlier times, further flattening the subhalo

merger rate slope. Second, there is a significant contribution of recently merged satellites to the merger population. We find that satellites are twice as likely to have had a recent merger as centrals of the same mass, regardless of mass cut and redshift (see §4 for more detail). This enhances the merger rate, with a stronger enhancement at later times since the satellite fraction grows with time as in Fig. 3.

At lower redshift, Fig. 4 (right) shows that the amplitude of the subhalo merger rate remains lower than that of halos, but the slopes become similar, indicating the effects examined above become less time-dependent. Since the masses we probe are crossing $M_*(t)$ as these redshifts, the reduced amplitude from subhalo vs. halo mass cut becomes less sensitive to time. Similarly, our mass range crossing $M_*(t)$ means that halo mass growth slows, so the fraction of halo major mergers that leads to subhalo major mergers remains roughly constant with time. Finally, as shown in Fig. 3, the satellite fraction growth asymptotes at lower redshift, which means that the enhancement from recently merged satellites remains roughly constant.

4 SATELLITE VS. CENTRAL MERGERS

The stereotypical galaxy merger is a satellite coalescing with the central in its halo and producing a central merger remnant. These mergers do dominate the merger population, both in parent types (central-satellite) and child type (cen-

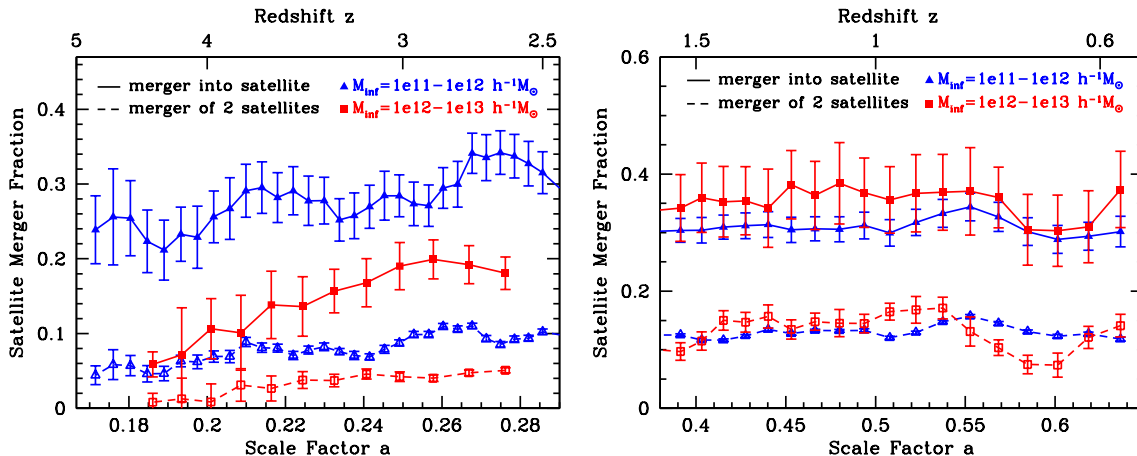


Figure 5. Satellite merger fraction at $z = 5 - 2.5$ (left) and $z = 1.6 - 0.6$ (right) for $M_{\text{inf}} = 10^{11} - 10^{12} h^{-1} M_{\odot}$ (triangles) and $M_{\text{inf}} = 10^{11} - 10^{12} h^{-1} M_{\odot}$ (squares). Closed point/solid lines indicate the fraction of all subhalo mergers that result in a satellite, while open points/dashed lines indicated the fraction of all subhalo mergers that arise from satellite-satellite parents.

tral). However, while satellites form the minority of the subhalo population at all epochs (see Fig. 3), satellites are twice as likely to have had a recent merger as centrals of the same mass, regardless of mass and redshift.

Since the identities of satellite vs. central subhalos at this mass and redshift regime are not clear-cut (from switches), we characterize mergers both in terms of their parent types (central/satellite) and resulting child types. For mergers resulting in centrals, this ambiguity is not important: 97% arise from satellite-central parents, while the other 3% arise from satellite-satellite parents during switches.¹⁵

Recently merged satellites are a more varied population. Figure 5 shows the contributions of satellite mergers to the overall merger populations as a function of the scale factor.¹⁶ The fraction of all subhalo mergers that result in a satellite is $\sim 30\%$ for $M_{\text{inf}} = 10^{11} - 10^{12} h^{-1} M_{\odot}$, with little dependence on redshift. For $M_{\text{inf}} = 10^{12} - 10^{13} h^{-1} M_{\odot}$ it is 15–20% at $z \sim 2.5$ and rises to $\sim 35\%$ at $z < 1.6$. Thus, at lower redshift ($z < 1.6$) where the satellite fraction asymptotes to $\sim 25\%$, the fraction of mergers that result in a satellite roughly reflects the satellite fraction as a whole.

Of these recently merged satellites, 20%–35% come from satellite-satellite parents within a single halo, while $\sim 7\%$ arise when a central-satellite merger occurs in a halo as it falls into a larger halo, becoming a satellite. The rest arise from switches, i.e. a satellite merges with a central, and the resulting subhalo no longer is the most massive subhalo, thus becoming a satellite. These switches occur primarily in halos only a few times more massive than the satellite, typically for satellites in close proximity to their central. At higher halo masses, recently merged satellites are dominated by satellite-satellite parents. These satellite-satellite mergers preferentially occur in the outer regions of a halo and are comparatively less common in the central regions.

¹⁵ A few percent arise from central-central parents, when the central regions of two halos coalesce so quickly that they are not seen as satellite-central subhalos given finite time resolution. We include these as satellite-central parents.

¹⁶ Satellite merger fractions are boxcar-averaged across three consecutive outputs to reduce noise from small number statistics.

We examine in more detail the environmental dependence of subhalo mergers in Wetzel et al. (2009).

Considering instead only parent types, Fig. 5 shows that 5–10% of all mergers come from satellite-satellite parents at $z \sim 2.5$, a fraction which increases to 10–15% at $z = 1.6$ and remains flat thereafter. Approximately 80% of all satellite-satellite mergers lead to a satellite child, while the rest lead to a central during a switch.

5 GALAXY AND HALO MERGER COUNTS

5.1 Counts of Recent Mergers

The distribution of the number of mergers per object within a fixed time interval gives the fraction of objects at a given epoch that might exhibit merger-related activity or morphological disturbance.¹⁷ Multiple mergers as well might contribute to specific properties, e.g., the formation and mass growth of elliptical galaxies (e.g., Boylan-Kolchin et al. 2005; Robertson et al. 2006; Naab et al. 2006; Conroy et al. 2007).

Figure 6 shows the fraction of subhalos at $z = 2.6$ and $z = 1$ with a given number of mergers in the last 1 Gyr. At $z = 2.6$, 30% of subhalos have suffered at least one major merger. Interestingly, this fraction is nearly constant across the mass regimes we probe. In contrast, the fraction of halos with at least one major merger within 1 Gyr is about twice as large, with stronger mass dependence: higher mass halos experience more mergers. At high redshift, halos are also significantly more likely to have undergone multiple mergers than subhalos, which builds up the satellite population.

At $z = 1$, recent mergers of subhalos and halos become less common, with only 8% of subhalos having suffered at least one major merger in the last 1 Gyr. Objects which have had 1 or 2 mergers are still more common for halos than subhalos, though high mass subhalos exhibit a much higher fraction of 3 or more mergers than halos of the same (infall)

¹⁷ This differs from the merger rates of §3, since we are tracking the histories of individual objects selected at a given redshift.

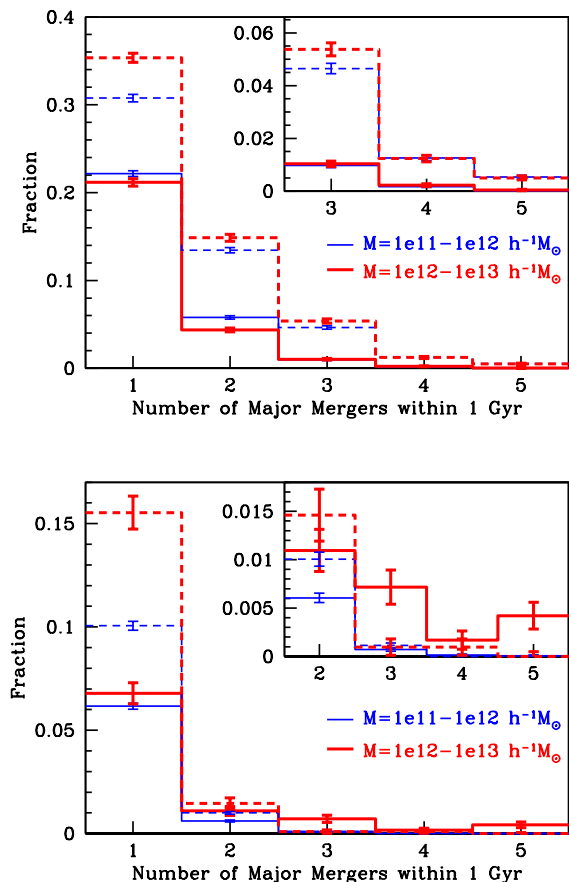


Figure 6. **Top:** Fraction of subhalos at $z = 2.6$ that have had a given number of mergers in the last 1 Gyr, for $M_{\text{inf}} = 10^{11} - 10^{12} h^{-1} M_{\odot}$ (thin lines) and $M_{\text{inf}} = 10^{12} - 10^{13} h^{-1} M_{\odot}$ (thick lines). Dashed lines show the same, but for host halos. 30% of subhalos have had at least one merger (independent of mass), while for halos this fraction is 50% (lower mass) and 57% (higher mass). Inset shows detail for > 2 mergers. **Bottom:** Same, but at $z = 1$. 8% of subhalos have had at least one merger (independent of mass), while for halos this fraction is 11% (lower mass) and 17% (higher mass). High mass subhalos show a much larger fraction of multiple mergers. Inset shows detail for > 1 merger.

mass. (Subhalos that have undergone 1 merger can be either satellites or centrals, those that have undergone 2 or more mergers are almost entirely centrals.) The build-up of the satellite population at higher redshift has allowed massive centrals to experience multiple mergers at lower redshift. This effect is stronger for more massive subhalos since they are more likely to be centrals, and they reside in higher mass halos with more massive satellites.

5.2 Fraction “On”

The fraction of halos that host recent mergers, f_{on} , is of particular interest for quasar or starburst evolution models, and quasar/starburst feedback effects such as heating of the Intracluster Medium (ICM). We select mergers up to 200 Myr after coalescence, motivated by the expected time interval during which quasars or starbursts remain observable (e.g., Hopkins et al. 2005). This time interval is only illustrative,

though, as one expects relevant lifetimes to depend strongly upon galaxy mass and merger ratio. Observables might depend upon dynamical time as well, although many quasar triggering effects might be related to microphysics—small scale interactions close to the merger—that do not evolve with time.¹⁸

Figure 7 shows the evolution of f_{on} for halos hosting subhalo mergers within the last 200 Myr. The same quantity is shown for halos with recent mergers themselves. At high redshift, f_{on} for halo mergers shows a steep decline from the decreasing halo merger rate. However, f_{on} for subhalo-subhalo mergers is flat from $z = 2.5 - 5$, because the subhalo merger rate per object decreases while the number of massive satellites in a given mass halo rises, causing the number of massive subhalo mergers within the halo to remain constant. At low redshift, where the satellite population grows more slowly, the evolution of this fraction for subhalo mergers more closely parallels that of halo mergers.

6 EVOLUTION OF THE SATELLITE HALO OCCUPATION

The redshift evolution of the satellite galaxy populations of dark matter halos is shaped by halo vs. galaxy mergers: halo mergers create satellites while galaxy mergers remove them.¹⁹ If the infall rate of satellites onto a halo is different than the satellite destruction rate, the satellite halo occupation will evolve with time.

As shown in Fig. 4, at $z > 2.5$, the merger rate of subhalos is significantly lower and shallower in slope than that of halos, implying that subhalos are being created faster than they are destroyed (at a rate decreasing with time). Conversely, at $z < 1.6$ the merger rates of halos and subhalos exhibit approximately the same redshift dependence, and their amplitudes are similar (also recall from §3 that not all halo major merger lead to subhalo major mergers). Thus, for halos of a fixed mass, we expect a rapid rise in the satellite halo occupation prior to $z \sim 2$ and a levelling-off with more gradual evolution at lower redshift.

6.1 Satellite Halo Occupation in Simulation

The above trends are seen in Fig. 8, which shows the evolution of the satellite occupation per halo, for satellites with $M_{\text{inf}} > 10^{11} h^{-1} M_{\odot}$ in the $100h^{-1}$ Mpc simulation. Satellite occupation counts are normalized using the last output at $z = 0.6$. More massive satellites ($M_{\text{inf}} > 10^{12} h^{-1} M_{\odot}$) have similar evolution, with a peak in the satellite halo occupation at $z \approx 2.5$. For a fixed satellite infall mass, less massive halos exhibit stronger satellite occupation evolution with redshift, leading to a more prominent peak.

¹⁸ If we scale our f_{on} time interval by the dynamical time, the slope of f_{on} becomes slightly shallower, but the qualitative results do not change.

¹⁹ Though if one applies a mass threshold to a population, this is not strictly true since mergers also scatter lower mass objects into the population.

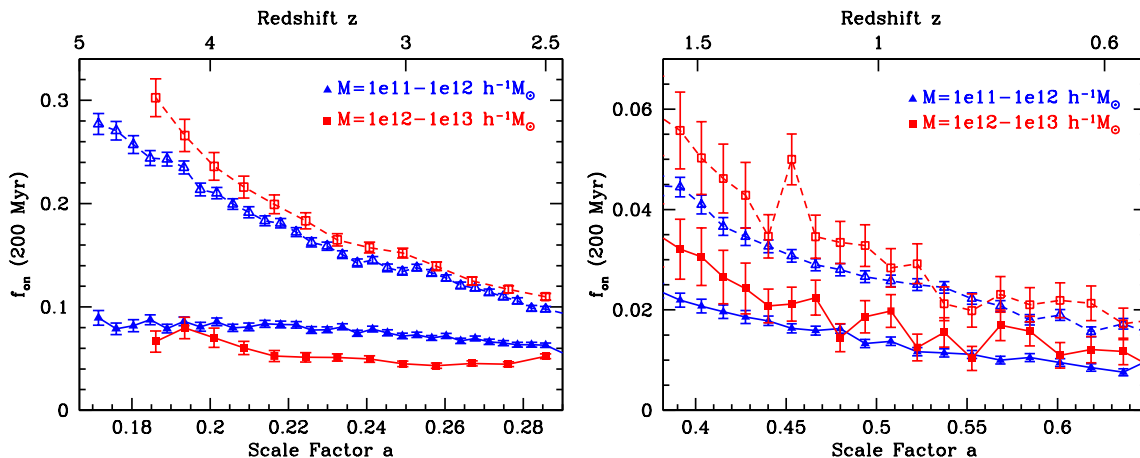


Figure 7. **Left:** Fraction of halos that host a subhalo-subhalo merger within the last 200 Myr (closed points/solid lines) at $z = 5 - 2.5$ for $M_{\text{inf}} = 10^{11} - 10^{12} h^{-1} M_{\odot}$ (triangles) and $M_{\text{inf}} = 10^{12} - 10^{13} h^{-1} M_{\odot}$ (squares). Open points/dashed lines show the fraction of halos of the same mass that have suffered a major halo-halo merger in the same time interval. **Right:** Same, but at $z = 1.6 - 0.6$.

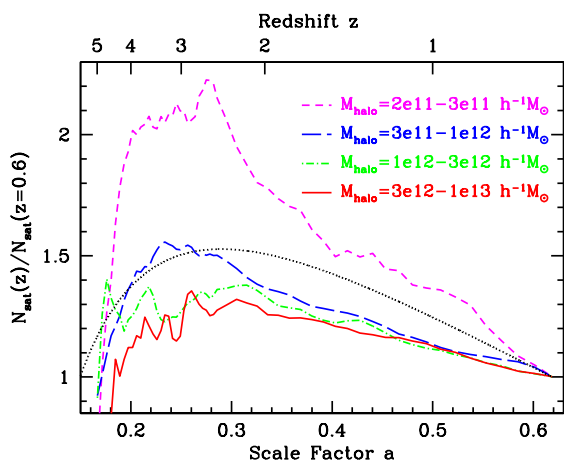


Figure 8. Evolution of the average number of satellite subhalos per halo for satellites with $M_{\text{inf}} > 10^{11} h^{-1} M_{\odot}$ and several halo mass bins. Satellite counts are normalized to those at $z = 0.6$ (the last output) and boxcar averaged across 3 outputs to reduce the small number statistics noise at early times. The dotted black line shows fit of Eq. 19 for 3:1 mass ratio mergers using halo merger rate parameters from Table 1. All halo masses have a peak in satellite occupation at $z \sim 2.5$, and similar trends persist for higher mass satellites. Less massive halos exhibit stronger evolution with redshift, leading to a more prominent peak.

6.2 Analytic Estimate of Satellite Halo Occupation

The rate of change of the satellite subhalo population per halo, for a fixed satellite M_{inf} , is given by the rate at which satellites fall into a halo (the halo merger rate) minus the rate at which satellites coalesce with the central subhalo

$$\frac{dN_{\text{sat}}}{dt} = \frac{dN_{\text{halo,merge}}}{dt} - \frac{dN_{\text{sat-cen,merge}}}{dt}. \quad (13)$$

The halo merger rate at all epochs is given by (§3)

$$\frac{dN_{\text{halo,merge}}}{dt} = A(1+z)^{\alpha} = Aa^{-\alpha} \quad (14)$$

The timescale for the satellite to coalesce with its central

subhalo after infall is given to good approximation by

$$t_{\text{sat-cen,merge}} \approx \frac{C_o}{10} \frac{M_{\text{halo}}/M_{\text{sat}}}{\ln(1 + M_{\text{halo}}/M_{\text{sat}})} t_{\text{Hubble}}. \quad (15)$$

where C_o is a constant of order unity that accounts for the ensemble averaged satellite orbital parameters, and we leave it as our sole free parameter. The rate of satellite destruction/coalescence is thus

$$\frac{dN_{\text{sat-cen,merge}}}{dt} = \frac{10}{C_o} \frac{\ln(1 + M_{\text{halo}}/M_{\text{sat}})}{M_{\text{halo}}/M_{\text{sat}}} H(z). \quad (16)$$

Combining Eqs. 14 and 16 into Eq. 13 one gets

$$\frac{dN_{\text{sat}}}{dt} = Aa^{-\alpha} - \frac{10}{C_o} \frac{\ln(1 + M_{\text{halo}}/M_{\text{sat}})}{M_{\text{halo}}/M_{\text{sat}}} H(z). \quad (17)$$

At high redshift, $H(z) \approx H_o(\Omega_{\text{m},o} a^{-3})^{\frac{1}{2}}$, where $H_o \simeq 0.1 h \text{ Gyr}^{-1}$, which implies

$$\frac{dN_{\text{sat}}}{dt} \approx Aa^{-\alpha} - \frac{1}{C_o} \frac{\ln(1 + M_{\text{halo}}/M_{\text{sat}})}{M_{\text{halo}}/M_{\text{sat}}} \Omega_{\text{m},o}^{\frac{1}{2}} a^{-\frac{3}{2}}. \quad (18)$$

Across all mass and redshift regimes, the power law index for halo mergers is $\alpha = 2 - 2.3$ (§3), and we find no additional dependence on merger mass ratio, suggesting a universal power law index.²⁰ Thus, the creation and destruction terms in Eq. 18 have differing dependencies on the scale factor, which implies they become equal at some redshift, where the satellite occupation per halo reaches a maximum.

Using the exact evolution of the Hubble parameter (in our cosmology) of $H(z) = H_o(\Omega_{\text{m},o} a^{-3} + \Omega_{\Lambda})^{1/2}$ in Eq. 17, and integrating over a , the full evolution of the satellite occupation per halo is

$$N_{\text{sat}}(a) = \frac{A}{H_o} \int da \frac{a^{-(\alpha+1)}}{H(z)} - \frac{10}{C_o} \frac{M_{\text{sat}}}{M_{\text{halo}}} \ln\left(1 + \frac{M_{\text{halo}}}{M_{\text{sat}}}\right) \ln(a) + K \quad (19)$$

where the constant K accounts for initial/final conditions.

²⁰ Though merger rates for more discrepant mass ratios have higher amplitudes, as given by Eq. 5.

Figure 8 shows the resultant $N_{\text{sat}}(a)$, normalized to the satellite occupation per halo at final output, using typical values for the halo merger rate from Table 1 ($A = 0.032$ and $\alpha = 2.3$). These values correspond to 3:1 mass ratio mergers, for satellites with $M_{\text{inf}} = 10^{11} h^{-1} M_{\odot}$ this gives $M_{\text{halo}} = 3 \times 10^{11} h^{-1} M_{\odot}$. While the fit of this model to the simulation results is not exact, it nicely reproduces the general trends, especially given the simplicity of the model, which ignores halo/central mass growth, satellite-satellite mergers, and switches. For instance, it correctly produces a lower peak in satellite occupation for halos with satellites of more discrepant mass ratios (more massive halos for a fixed satellite mass, or less massive satellites for a fixed halo mass), relative to the amplitude at low redshift. This is because the decreased infall times for smaller satellite-halo mass ratios cause a more dramatic fall (after the peak) in the satellite population for lower mass halos.

Agreement of this model with our simulations also requires $C_o \approx 2$, which can be compared with other work. Zentner et al. (2005) and Jiang et al. (2008) find that the ensemble averaged satellite orbital circularity distribution is given by $\langle \epsilon \rangle = 0.5 \pm 0.2$, with no strong dependence on redshift or satellite-halo mass ratio. When applied to detailed dynamical friction timescale fits from simulation, this yields $C_o \approx 0.6$ (Boylan-Kolchin et al. 2008) and $C_o \approx 1.4$ (Jiang et al. 2008).²¹ Taken at face value, our even higher value of C_o means that our satellites are taking longer to merge, suggesting that the discrepancy does not arise from artificial over-merging in our simulations. However, exact comparisons are difficult given the simple nature of our analytic model, and because both of these groups use different halo and subhalo finding algorithms. Jiang et al. (2008), who used a simulation of roughly similar volume and mass resolution to ours, also incorporated hydrodynamics, which is likely to shorten the merger timescale since it introduces further dissipational effects to the subhalo orbits and reduces mass loss. Compared with Boylan-Kolchin et al. (2008), who performed much higher resolution simulations of isolated halo mergers, it is possible that our satellite subhalos experience more severe mass stripping upon infall, decreasing their mass and thus extending their subsequent infall time (see Eq. 8). A more detailed investigation of satellite infall timescales in a cosmological setting is needed, studies now in progress are targeting in particular the role of hydrodynamic effects (Dolag et al. 2008; Saro et al. 2008; Simha et al. 2008).

6.3 Comparison to Other Work on Satellite Occupation Evolution

Figure 8 shows a peak in the number of satellites per halo at $z \sim 2.5$. Fundamentally, the reason for this peak is that we select subhalos of *fixed* minimum *infall* mass in halos of *fixed* mass across time. If instead we examine the satellite occupation for halos above a minimum mass cut, the growth of massive halos (hosting more satellites) at late time would overwhelm the drop in the satellite population at a fixed halo

mass, so the satellite halo occupation would grow monotonically and appear much like the satellite fraction in Fig. 3, which ignores halo mass.²²

These results agree with the interpretation that more massive halos have later formation times and longer satellite infall times, and thus host more substructure at a given epoch (van den Bosch et al. 2005; Zentner et al. 2005). Similarly, for a fixed satellite infall mass, the satellite halo occupation evolves more rapidly for less massive halos, as Zentner et al. (2005) and Diemand et al. (2007) found, though their results were based upon subhalo instantaneous mass and maximum circular velocity (we compare these to M_{inf} in the Appendices).

However, the peak in satellite halo occupation in Fig. 8 does not appear in Halo Occupation Distribution (HOD) evolution studies by Zentner et al. (2005) because they use a fixed cut on instantaneous maximum circular velocity across time. As shown in Appendix A, fixed $V_{c,\text{max}}$ probes lower mass at higher redshift, and this evolution in satellite mass overwhelms the satellite evolution of Fig. 8, leading to a monotonic rise in the satellite halo occupation with redshift. Similarly, Conroy et al. (2006) noted that the HOD shoulder (the halo mass where a halo hosts only a central galaxy) becomes shorter at higher redshift as an increasing fraction of low-mass halos host more than one galaxy, finding a monotonically increasing satellite population with redshift. However, they compare fixed satellite number density (not mass) across redshift, which corresponds to a lower subhalo mass at higher redshift. Again, this overwhelms the evolution of Fig. 8, leading to a monotonic rise in the satellite population per halo with redshift.

In their semi-analytic model matched to simulation, van den Bosch et al. (2005) find that the average subhalo mass fraction of a halo always decreases with time, and they claim that, as a result, the timescale for subhalo mass loss (approximately the dynamical/infall time) is always smaller than the timescale of halo mass accretion (mergers). This implies that the satellite infall rate is always higher than the halo merger rate, and so the satellite HOD always decreases with time. However, this result refers to the total subhalo instantaneous mass per halo, not galaxy counts based on infall mass. If instead we examine the evolution of the satellite occupation per halo as in Fig. 8 selecting the satellites based on *instantaneous* subhalo mass instead of infall mass, we find a monotonic increase in the satellite occupation with no peak, in agreement with other authors above.

These examples all illustrate how the evolution of the HOD is dependent both on satellite mass assignment and selection of fixed mass vs. circular velocity vs. number density across time.

7 SUMMARY AND DISCUSSION

Using high-resolution dark matter simulations in cosmological volumes, we have measured the rates, counts, and types of subhalo (galaxy) major mergers at redshift $z = 0.6 - 5$, describing their populations in terms of centrals/satellites

²¹ The C_o values of these two fits agree only in extreme cases, i.e. maximally circular orbits for Boylan-Kolchin et al. (2008) or maximally eccentric orbits for (Jiang et al. 2008).

²² Though the satellite halo occupation would have a higher amplitude since it measures $n_{\text{sat}}/n_{\text{central}}$ while the satellite fraction measures $n_{\text{sat}}/n_{\text{subhalo}} = n_{\text{sat}}/(n_{\text{central}} + n_{\text{sat}})$.

and contrasting their merger properties with those of halos of the same (infall) mass. We assign subhalos their mass at infall (with the capacity for mass growth during satellite mergers), motivated by an expected correlation with galaxy stellar mass, but include no further semi-analytic galaxy modelling. We select mergers requiring 3:1 or closer infall mass ratios, motivated by the expectation that these can trigger activity such as quasars, starbursts, and related objects such as Lyman break galaxies, submillimeter galaxies, and ULIRGs. We highlight our main results as follows:

- The merger rate per object of subhalos is always lower than that of halos of the same (infall) mass. Galaxies exhibit stronger mass dependence on the amplitude of their merger rate than halos, with more massive galaxies undergoing more mergers. While the slope of the halo merger rate per object is essentially redshift independent, the slope of the galaxy merger rate is much shallower than that of halos at $z > 2.5$ and parallels that of halos at $z < 1.6$.

- These differences in halos and subhalo merger rates arise because (1) halo mergers add mass to halos instantly, while central subhalo mass grows more gradually after a halo merger; (2) halo major mergers do not necessarily lead to subhalo major mergers, since central subhalos experience mass growth while a satellite subhalo's infall mass typically remains constant as it orbits; and (3) the satellite subhalo fraction grows with time, and satellites are twice as likely to be recent mergers as centrals of the same infall mass.

- 15%–35% of all recently merged subhalos are satellites, though a significant fraction of these arise from satellite-central parents during switches. 5%–15% of galaxy mergers arise from satellite-satellite parents, with a higher fraction at lower redshift.

- At $z = 2.6$ ($z = 1$), 30% (8%) of galaxies have experience at least one major merger in the last 1 Gyr, regardless of mass. Halos are more likely to have experience multiple mergers in their recent history.

- The likelihood of a halo to host a recently merged galaxy, f_{on} , does not evolve with time at $z > 2.5$ and falls with time at $z < 1.6$.

- Comparing galaxy and halo merger rates allows one to understand the evolution of the satellite halo occupation, and we approximated this behaviour analytically including fits to our simulations. Selecting subhalos on fixed infall mass, the satellite halo occupation for halos of a fixed mass increases with time at high redshift, peaks at $z \sim 2.5$, and falls with time after that. This implies similar evolution for the satellite galaxy component of the Halo Occupation Distribution.

Our results, based entirely on the dynamics of dark matter, represent an important but preliminary step towards quantifying the nature of galaxy mergers in hierarchical structure formation. To compare to many observables we would need to include baryonic effects, and indeed such effects can provide corrections to the merger rates themselves (Dolag et al. 2008; Jiang et al. 2008; Saro et al. 2008). The merger rates here also do not include whether the subhalos are gas-rich (required for some observables) or not, though at the high redshifts we examine, we expect almost all galaxies to be gas-rich. While satellites can be stripped of much of their gas before merging with their central (e.g., Dolag et al. 2008; Saro et al. 2008), we have considered primarily mas-

sive satellites (relative to their host halos), which have short infall times and thus experience less gas stripping.

Timescales between observables and our measured merger event also play a role. In simulations, a quasar can appear up to ~ 1 Gyr after galaxy coalescence, though starbursts may occur more quickly (e.g., Hopkins et al. 2005; Springel et al. 2005; Cox et al. 2008). However, morphological disturbance is clearest during first passage and final coalescence (Lotz et al. 2008). The time scales for each signature to commence and/or persist also have a large scatter, ranging from 0.2 to 1.2 Gyr after the merger. Finally, specific observations will also have specific selection functions. The quantitative measurements provided here provide starting points for these analyses in addition to helping to understand the properties of galaxies and their mergers in general.

Unfortunately, our predictions are not easily compared to observations which estimate merger rates at $z \lesssim 1$ using close galaxy pairs or disturbed morphologies (most recently, Bell et al. 2006; Kampczyk et al. 2007; Kartaltepe et al. 2007; Lin et al. 2008; Lotz et al. 2008; McIntosh et al. 2008; Patton & Atfield 2008) since they have found that the close pair fraction evolves as $(1+z)^\alpha$ with a diverse range of exponents from $\alpha = 0$ to 4. Furthermore, translating these observations into galaxy or halo merger rates requires including more physical effects, e.g. time dependent galaxy coalescence timescales (Kitzbichler & White 2008; Mateus 2008) or inclusion of changes in numbers of host halos with redshift (Berrier et al. 2006).

While we were preparing this work for preparation, Simha et al. (2008) appeared which considers detailed merger properties of satellite subhalos in a hydrodynamic simulation, and Angulo et al. (2008) appeared which considers satellite mergers in the Millennium simulation. After this paper was submitted, Stewart et al. (2008) appeared, which also considers merger rates as a function of mass, redshift, and mass ratio.

ACKNOWLEDGMENTS

We thank E. Scannapieco and K. Stewart for useful conversations and thank CCAPP at the Ohio State University for hospitality and hosting a meeting which started this project. We also thank the referee for several useful suggestions. A.W. gratefully acknowledges the support of an NSF Graduate Fellowship, J.D.C. support from NSF-AST-0810820 and DOE, and M.W. support from NASA and the DOE. The simulations were analyzed at the National Energy Research Scientific Computing Center.

APPENDIX A: SUBHALO MASS AND CIRCULAR VELOCITY

Here we further elaborate on the details of subhalos in our simulations, including their radial density and circular velocity profiles and the relation between mass and maximal circular velocity, including its evolution with time.

Figure A1 shows the radial density and circular velocity profiles for 8 satellite and 8 central subhalos with $V_{c,\text{max}} \simeq 250$ km/s ($M \sim 10^{12} h^{-1} M_\odot$) at $z = 2.6$ in the $100h^{-1}$ Mpc simulation. Circular velocity is defined as

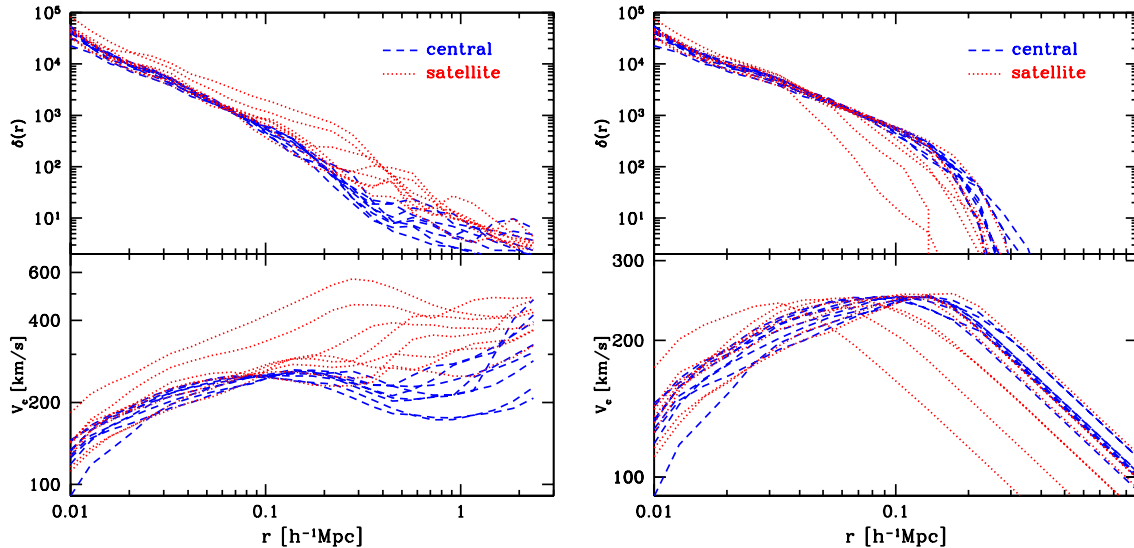


Figure A1. Left: Radial density profiles (top) and circular velocity profiles (bottom) of all matter around 8 satellite (dotted) and 8 central (dashed) subhalos with $V_{c,\text{max}} \simeq 250$ km/s at $z = 2.6$. Right: Same, but only for matter assigned to the subhalos.

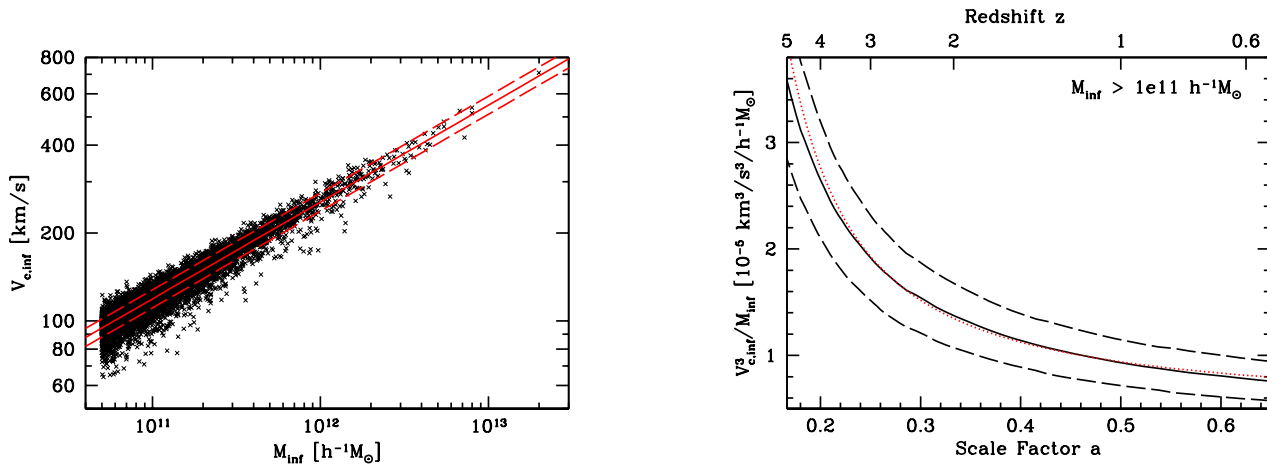


Figure A2. Relation between subhalo infall maximum circular velocity, $V_{c,\text{inf}}$, and subhalo infall mass, M_{inf} , at $z = 2.6$. Black points show a 25% sub-sample of all subhalos as a measure of scatter, the solid red line shows the least squares fit to Eq. A1, and the dashed red lines show the 1σ scatter, for subhalos with $M_{\text{inf}} > 10^{11} h^{-1} M_\odot$.

$V_c \equiv \sqrt{GM(<r)}/r$, and since subhalos follow NFW density profiles, with a break in the power-law density profile at the scale radius, r_s , they have a maximum value in their circular velocity profiles, $V_{c,\text{max}}$, at $r_{\text{max}} = 2.2r_s$. The left panels show the radial profiles of all matter surrounding the subhalos, while the right panels show only that of matter assigned to the subhalos. Satellites and centrals have similar profiles at small radii, though the right top panel shows that satellites exhibit signs of tidal truncation at $\sim 50h^{-1}$ kpc. This is also visible in the circular velocity profile in the bottom left panel, where V_c for satellites rises sharply, exhibiting a transition to their host halos. For the centrals, the rise in V_c beyond $\sim 1h^{-1}$ Mpc arises from neighbouring structures.

Figure A2 shows the relation between subhalo infall

Figure A3. Evolution of the ratio of subhalo infall maximum circular velocity to infall mass, $B(z) = V_{c,\text{inf}}^3/M_{\text{inf}}$ (solid), and 1σ scatter (dashed) for subhalos with $M_{\text{inf}} > 10^{11} h^{-1} M_\odot$. Dotted line shows fit to $B(z)$ of Eq. A2.

mass, M_{inf} , and infall maximum circular velocity, $V_{c,\text{inf}}$, for subhalos at $z = 2.6$. We fit this relation to

$$V_{c,\text{inf}}^\gamma = B(z)M_{\text{inf}} \quad (\text{A1})$$

for all subhalos above $10^{11} h^{-1} M_\odot$, finding $\gamma = 3$ holds to good approximation at all redshifts we examine, in agreement with the virial relation $V_{c,\text{max}}^2 \propto M/R \propto M/M^{1/3} \propto M^{2/3}$. The outliers with large M_{inf} relative to $V_{c,\text{inf}}$ are satellites that experienced a major merger; under our prescription, a satellite child's M_{inf} is the sum of its parents' M_{inf} , but a child's $V_{c,\text{inf}}$ is that of its highest $V_{c,\text{inf}}$ parent.

Fixing $\gamma = 3$, Fig. A3 shows the evolution of the amplitude $B(z) \equiv V_{c,\text{inf}}^3/M_{\text{inf}}$. A subhalo of a given mass has a higher maximum circular velocity at higher redshift, reflective of the increased density of the universe when the subhalo formed. As a subhalo subsequently accretes mass,

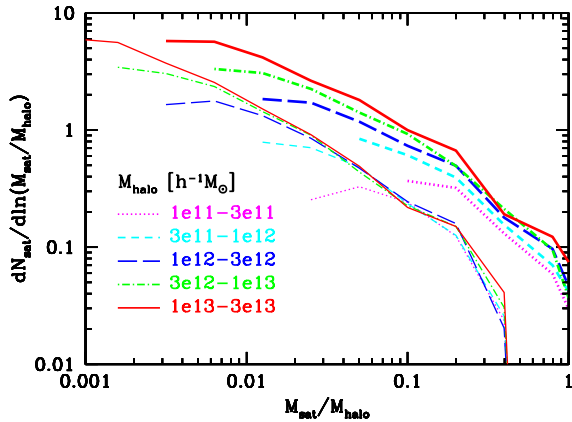


Figure B1. Satellite subhalo (scaled) mass function, for various host halo mass bins, at $z = 1$. Thick curves show satellite mass selected on M_{inf} , while thin curves show satellite mass selected on instantaneous bound mass. While the instantaneous bound mass function exhibits no dependence on halo mass, the infall mass function has a higher amplitude for more massive halos. An appreciable number of satellites exists at $M_{\text{sat,inf}}/M_{\text{halo}} \approx 1$ because of switches. Below the rollover at high satellite mass, both mass functions scale as $\frac{dN_{\text{sat}}}{d \ln(M_{\text{sat}}/M_{\text{halo}})} \propto M_{\text{sat}}^{-0.9}$ in agreement with instantaneous satellite subhalo bound mass functions found by numerous authors (see text).

its $V_{\text{c,max}}^3$ grows more slowly than its mass (in cases of slow mass growth, we find $V_{\text{c,max}}^3$ can remain constant). This is in agreement with Diemand et al. (2007), who found that halos undergoing mild mass growth (no major mergers) had less than 10% change in $V_{\text{c,max}}$ and r_{max} . We find that the evolution of $B(z)$ (within the redshifts we probe) can be well-approximated by

$$B(z) = 6.56 \times 10^{-6} e^{0.36z} (\text{km/s})^3 h M_{\odot}^{-1}. \quad (\text{A2})$$

Thus, $M_{\text{inf}} = 10^{11}$ (10^{12}) $h^{-1} M_{\odot}$ subhalos correspond to $V_{\text{c,inf}} \simeq 120$ (250) km/s at $z = 2.6$ and $V_{\text{c,inf}} \simeq 100$ (200) km/s at $z = 1$. Conversely, for fixed $V_{\text{c,inf}}$, a subhalo is about half as massive at $z = 2.6$ than at $z = 1$.

Since we fit relations of satellite subhalo properties at infall, our results above are applicable equally to satellite and central subhalos. In addition, our results change by only a few percent if we instead consider host halos.

APPENDIX B: SATELLITE SUBHALO MASS FUNCTION

Figure B1 shows the satellite subhalo (scaled) mass function vs. the ratio of satellite mass to halo mass, for various host halo mass bins at $z = 1$. Thick curves show satellite masses selected on M_{inf} , while thin curves show satellite masses selected on instantaneous bound mass. The rollover in the M_{inf} curves at low satellite mass indicates where satellites become numerically disrupted by resolution effects. Numerical disruption occurs at higher satellite M_{inf} for more massive halos, indicating that satellites of a fixed M_{inf} experience more pronounced tidal stripping in higher mass halos, where dynamical friction timescales and central densities are higher. The rollover in the highest halo mass bin occurs at

$M_{\text{sat,inf}} \approx 10^{11} h^{-1} M_{\odot}$, which sets our minimum subhalo mass for robust tracking.

We find that the scaled instantaneous bound mass function exhibits little-to-no systematic dependence on halo mass, in agreement with Angulo et al. (2008).²³ This is in contrast to the scaled infall mass function, which shows more satellites at a given mass ratio for more massive halos. This difference is driven by subhalo mass stripping. Averaged over the entire satellite population at this redshift, the satellite instantaneous bound mass is $\sim 30\%$ that of M_{inf} , as can be seen by the x-axis offset of the solid and dashed curves. However, satellites exhibit less average mass loss in low-mass halos than high-mass halos, the instantaneous to infall mass ratios being 40% and 25%, respectively. This is considerably higher than the 5% – 10% at $z = 1$ found in the semi-analytic model of van den Bosch et al. (2005). Additionally van den Bosch et al. (2005) and Giocoli et al. (2008) found the opposite trend with halo mass, i.e., that the average mass loss of satellites is higher for lower mass halos. They find that this arises because lower mass halos form (and accrete their subhalos) earlier, when the dynamical/stripping timescale is shorter. Thus, the satellites of lower mass halo are stripped both more rapidly and over a longer time period (see also Zentner et al. 2005). Finally, Giocoli et al. (2008) find that the scaled mass functions of subhalos at infall does not depend on halo mass, in seeming contrast with Fig. B1.

These discrepancies likely arise because we examine the masses of extant subhalos in our simulation, while van den Bosch et al. (2005) and Giocoli et al. (2008) track subhalo mass loss much longer than our simulation does. Their semi-analytical model of subhalo mass loss has no prescription for central-satellite mergers, which preferentially serve to reduce highly stripped satellites from our sample.²⁴ Since satellites of a given infall mass to halo mass ratio have lower mass in lower mass halos, they are closer to our minimum subhalo finding mass threshold. Thus, a fixed amount of stripping will cause lower mass halos to have a reduced population of satellites of a given infall mass to halo mass ratio. It is unclear at what level of subhalo mass stripping we should expect the galaxies they host to become disrupted as well.

Various studies using high resolution simulations have explored in detail the slope of the subhalo mass function (De Lucia et al. 2004; Gao et al. 2004; Diemand et al. 2007; Madau et al. 2008; Angulo et al. 2008), finding that the (instantaneous) mass function of subhalos goes as $N_{\text{sat}}(> M_{\text{sat}}) \propto (M_{\text{halo}}/M_{\text{sat}})^{\alpha}$, with $\alpha = 0.9 - 1$.²⁵ We note, though, that these fits are based on cuts on instantaneous subhalo mass or circular velocity, not those at infall. However, we find that, between the rollover in M_{inf} at low and high satellite mass, the slopes of the mass functions selected on infall and instantaneous bound mass are the same within error, and $\alpha = 0.9$ fits our mass function selected on either mass. The similarity of the two slopes also implies that

²³ We thank the referee for suggesting we show this quantity.

²⁴ See Taylor & Babul (2005) and Zentner et al. (2005) for detailed comparisons of simulated subhalos with analytic models.

²⁵ $N_{\text{sat}}(> M_{\text{sat}})$ has the same power law dependence on subhalo mass as $\frac{dN_{\text{sat}}}{d \ln(M_{\text{sat}}/M_{\text{halo}})}$.

the mass loss rate of satellites does not depend strongly on satellite mass, in agreement with Giocoli et al. (2008).

REFERENCES

- Allgood B., Flores R. A., Primack J. R., Kravtsov A. V., Wechsler R. H., Faltenbacher A., Bullock J. S., 2006, *MNRAS*, 367, 1781
- Allgood B. A., 2005, PhD thesis, University of California, nta Cruz, United States – California
- Angulo R. E., Lacey C. G., Baugh C. M., Frenk C. S., 2008, ArXiv e-prints 0810.2177
- Barnes J. E., Hernquist L. E., 1991, *ApJ*, 370, L65
- Bell E. F., Phleps S., Somerville R. S., Wolf C., Borch A., Meisenheimer K., 2006, *ApJ*, 652, 270
- Benson A. J., Kamionkowski M., Hassani S. H., 2005, *MNRAS*, 357, 847
- Berlind A. A., Weinberg D. H., 2002, *ApJ*, 575, 587
- Berrier J. C., Bullock J. S., Barton E. J., Guenther H. D., Zentner A. R., Wechsler R. H., 2006, *ApJ*, 652, 56
- Binney J., Tremaine S., 2008, *Galactic Dynamics: Second Edition*. Princeton University Press, Princeton, NJ
- Blain A. W., Smail I., Ivison R. J., Kneib J.-P., Frayer D. T., 2002, *Phys. Rep.*, 369, 111
- Blumenthal G. R., Faber S. M., Flores R., Primack J. R., 1986, *ApJ*, 301, 27
- Bower R. G., Benson A. J., Malbon R., Helly J. C., Frenk C. S., Baugh C. M., Cole S., Lacey C. G., 2006, *MNRAS*, 370, 645
- Boylan-Kolchin M., Ma C.-P., Quataert E., 2005, *MNRAS*, 362, 184
- Boylan-Kolchin M., Ma C.-P., Quataert E., 2008, *MNRAS*, 383, 93
- Carlberg R. G., 1990, *ApJ*, 350, 505
- Cohn J. D., Bagla J. S., White M., 2001, *MNRAS*, 325, 1053
- Cohn J. D., White M., 2005, *Astroparticle Physics*, 24, 316
- Cohn J. D., White M., 2008, *MNRAS*, 385, 2025
- Conroy C., Ho S., White M., 2007, *MNRAS*, 379, 1491
- Conroy C., Wechsler R. H., 2008, arXiv: 0805.3346
- Conroy C., Wechsler R. H., Kravtsov A. V., 2006, *ApJ*, 647, 201
- Cooper M. C., Newman J. A., Coil A. L., Croton D. J., Gerke B. F., Yan R., Davis M., Faber S. M., Guhathakurta P., Koo D. C., Weiner B. J., Willmer C. N. A., 2007, *MNRAS*, 376, 1445
- Cooray A., Sheth R., 2002, *Phys. Rep.*, 372, 1
- Coppin K., Chapin E. L., Mortier A. M. J., Scott S. E., Borys C., Dunlop J. S., Halpern M., Hughes D. H., Pope A., Scott D., Serjeant S., et al., 2006, *MNRAS*, 372, 1621
- Cox T. J., Jonsson P., Somerville R. S., Primack J. R., Dekel A., 2008, *MNRAS*, 384, 386
- Davis M., Efstathiou G., Frenk C. S., White S. D. M., 1985, *ApJ*, 292, 371
- De Lucia G., Kauffmann G., Springel V., White S. D. M., Lanzoni B., Stoehr F., Tormen G., Yoshida N., 2004, *MNRAS*, 348, 333
- Dekel A., Devor J., Hetzroni G., 2003, *MNRAS*, 341, 326
- Diemand J., Kuhlen M., Madau P., 2007, *ApJ*, 667, 859
- Diemand J., Moore B., Stadel J., 2004, *MNRAS*, 352, 535
- Dolag K., Borgani S., Murante G., Springel V., 2008, arXiv: 0808.3401
- Dubinski J., 1994, *ApJ*, 431, 617
- Evrard A. E., Bialek J., Busha M., White M., Habib S., Heitmann K., Warren M., Rasia E., Tormen G., Moscardini L., Power C., Jenkins A. R., Gao L., Frenk C. S., Springel V., White S. D. M., Diemand J., 2008, *ApJ*, 672, 122
- Fakhouri O., Ma C.-P., 2008, *MNRAS*, 386, 577
- Faltenbacher A., Allgood B., Gottlöber S., Yepes G., Hoffman Y., 2005, *MNRAS*, 362, 1099
- Gao L., De Lucia G., White S. D. M., Jenkins A., 2004, *MNRAS*, 352, L1
- Gao L., White S. D. M., Jenkins A., Stoehr F., Springel V., 2004, *MNRAS*, 355, 819
- Gawiser E., Francke H., Lai K., Schawinski K., Gronwall C., Ciardullo R., Quadri R., Orsi A., Barrientos L. F., et al., 2007, *ApJ*, 671, 278
- Genel S., Genzel R., Bouché N., Sternberg A., Naab T., Schreiber N. M. F., Shapiro K. L., Tacconi L. J., Lutz D., Cresci G., Buschkamp P., Davies R. I., Hicks E. K. S., 2008, *ApJ*, 688, 789
- Gerke B. F., Newman J. A., Faber S. M., Cooper M. C., Croton D. J., Davis M., Willmer C. N. A., Yan R., Coil A. L., Guhathakurta P. and Koo D. C., Weiner B. J., 2007, *MNRAS*, 376, 1425
- Ghigna S., Moore B., Governato F., Lake G., Quinn T., Stadel J., 1998, *MNRAS*, 300, 146
- Ghigna S., Moore B., Governato F., Lake G., Quinn T., Stadel J., 2000, *ApJ*, 544, 616
- Giavalisco M., 2002, *ARA&A*, 40, 579
- Giocoli C., Tormen G., van den Bosch F. C., 2008, *MNRAS*, 386, 2135
- Gnedin O. Y., Ostriker J. P., 1997, *ApJ*, 474, 223
- Gottlöber S., Klypin A., Kravtsov A. V., 2001, *ApJ*, 546, 223
- Guo Q., White S. D. M., 2008, *MNRAS*, 384, 2
- Harker G., Cole S., Helly J., Frenk C., Jenkins A., 2006, *MNRAS*, 367, 1039
- Heitmann K., Lukić Z., Fasel P., Habib S., Warren M. S., White M., Ahrens J., Ankeny L., Armstrong R., O’Shea B., Ricker P. M., Springel V., Stadel J., Trac H., 2008, *Computational Science and Discovery*, 1, 015003
- Hopkins P. F., Cox T. J., Kereš D., Hernquist L., 2008, *ApJS*, 175, 390
- Hopkins P. F., Hernquist L., Cox T. J., Di Matteo T., Martini P., Robertson B., Springel V., 2005, *ApJ*, 630, 705
- Hopkins P. F., Hernquist L., Cox T. J., Kereš D., 2008, *ApJS*, 175, 356
- Jiang C. Y., Jing Y. P., Faltenbacher A., Lin W. P., Li C., 2008, *ApJ*, 675, 1095
- Kampeczyk P., Lilly S. J., Carollo C. M., Scarlata C., Feldmann R., Koekemoer A., Leauthaud A., Sargent M. T., Taniguchi Y., Capak P., 2007, *ApJS*, 172, 329
- Kartaltepe J. S., Sanders D. B., Scoville N. Z., Calzetti D., Capak P., Koekemoer A., Mobasher B., Murayama T., Salvato M., Sasaki S. S., Taniguchi Y., 2007, *ApJS*, 172, 320
- Kauffmann G., White S. D. M., 1993, *MNRAS*, 261, 921
- Kitzbichler M. G., White S. D. M., 2008, *MNRAS*, 391, 1489
- Klypin A., Gottlöber S., Kravtsov A. V., Khokhlov A. M.,

- 1999, *ApJ*, 516, 530
- Kolatt T. S., Bullock J. S., Sigad Y., Kravtsov A. V., Klypin A. A., Primack J. R., Dekel A., 2000, *ArXiv Astrophysics e-prints* 0010222
- Komatsu E., Dunkley J., Nolta M. R., Bennett C. L., Gold B., Hinshaw G., Jarosik N., Larson D., Limon M., Page L., Spergel D. N., Halpern M., Hill R. S., Kogut A., Meyer S. S., Tucker G. S., Weiland J. L., Wollack E., Wright E. L., 2009, *ApJS*, 180, 330
- Kravtsov A. V., Berlind A. A., Wechsler R. H., Klypin A. A., Gottlöber S., Allgood B., Primack J. R., 2004, *ApJ*, 609, 35
- Lacey C., Cole S., 1993, *MNRAS*, 262, 627
- Lacey C., Cole S., 1994, *MNRAS*, 271, 676
- Li Y., Mo H. J., van den Bosch F. C., Lin W. P., 2007, *MNRAS*, 379, 689
- Lin L., Patton D. R., Koo D. C., Casteels K., Conselice C. J., Faber S. M., Lotz J., Willmer C. N. A., Hsieh B. C., Chiueh T., Newman J. A., Novak G. S., Weiner B. J., Cooper M. C., 2008, *ApJ*, 681, 232
- Lotz J. M., Davis M., Faber S. M., et al., 2008, *ApJ*, 672, 177
- Lotz J. M., Jonsson P., Cox T. J., Primack J. R., 2008, *MNRAS*, 391, 1137
- Madau P., Diemand J., Kuhlen M., 2008, *ApJ*, 679, 1260
- Maller A. H., Katz N., Kereš D., Davé R., Weinberg D. H., 2006, *ApJ*, 647, 763
- Mateus A., 2008, *arXiv: 0802.2720*
- Maulbetsch C., Avila-Reese V., Colín P., Gottlöber S., Khalatyan A., Steinmetz M., 2007, *ApJ*, 654, 53
- McIntosh D. H., Guo Y., Hertzberg J., Katz N., Mo H. J., van den Bosch F. C., Yang X., 2008, *MNRAS*, 388, 1537
- McLure R. J., Cirasuolo M., Dunlop J. S., Foucaud S., Almaini O., 2008, *arXiv: 0805.1335*
- Mo H. J., Mao S., White S. D. M., 1998, *MNRAS*, 295, 319
- Moore B., Ghigna S., Governato F., Lake G., Quinn T., Stadel J., Tozzi P., 1999, *ApJ*, 524, L19
- Murali C., Katz N., Hernquist L., Weinberg D. H., Davé R., 2002, *ApJ*, 571, 1
- Naab T., Khochfar S., Burkert A., 2006, *ApJ*, 636, L81
- Navarro J. F., Frenk C. S., White S. D. M., 1996, *ApJ*, 462, 563
- Neto A. F., Gao L., Bett P., Cole S., Navarro J. F., Frenk C. S., White S. D. M., Springel V., Jenkins A., 2007, *MNRAS*, 381, 1450
- Noguchi M., 1991, *MNRAS*, 251, 360
- Ouchi M., Shimasaku K., Okamura S., Furusawa H., Kashikawa N., Ota K., Doi M., Hamabe M., Kimura M., Komiyama Y., Miyazaki M., Miyazaki S., Nakata F., Sekiguchi M., Yagi M., Yasuda N., 2004, *ApJ*, 611, 660
- Patton D. R., Atfield J. E., 2008, *ApJ*, 685, 235
- Peacock J. A., Smith R. E., 2000, *MNRAS*, 318, 1144
- Percival W., Miller L., 1999, *MNRAS*, 309, 823
- Reed D., Governato F., Quinn T., Gardner J., Stadel J., Lake G., 2005, *MNRAS*, 359, 1537
- Reichardt C. L., Ade P. A. R., Bock J. J., Bond J. R., Brevik J. A., Contaldi C. R., Daub M. D., Dempsey J. T., Goldstein J. H., Holzappel W. L., Kuo C. L., Lange A. E., Lueker M., Newcomb M., Peterson J. B., Ruhl J., Runyan M. C., Staniszewski Z., 2008, *arXiv: 0801.1491*
- Robertson B., Cox T. J., Hernquist L., Franx M., Hopkins P. F., Martini P., Springel V., 2006, *ApJ*, 641, 21
- Sanders D. B., Mirabel I. F., 1996, *ARA&A*, 34, 749
- Saro A., De Lucia G., Dolag K., Borgani S., 2008, *MNRAS*, 391, 565
- Seljak U., 2000, *MNRAS*, 318, 203
- Sheth R. K., Tormen G., 1999, *MNRAS*, 308, 119
- Simha V., Weinberg D. H., Dave R., Gnedin O. Y., Katz N., Keres D., 2008, *arXiv: 0809.2999*
- Smoot G. F., et al., 1992, *ApJ*, 396, L1
- Somerville R. S., Lemson G., Kolatt T. S., Dekel A., 2000, *MNRAS*, 316, 479
- Springel V., Di Matteo T., Hernquist L., 2005, *MNRAS*, 361, 776
- Springel V., White S. D. M., Jenkins A., Frenk C. S., Yoshida N., Gao L., Navarro J., Thacker R., Croton D., Helly J., Peacock J. A., Cole S., Thomas P., Couchman H., Evrard A., Colberg J., Pearce F., 2005, *Nature*, 435, 629
- Springel V., White S. D. M., Tormen G., Kauffmann G., 2001, *MNRAS*, 328, 726
- Steidel C. C., Adelberger K. L., Shapley A. E., Pettini M., Dickinson M., Giavalisco M., 2003, *ApJ*, 592, 728
- Stewart K. R., Bullock J. S., Barton E. J., Wechsler R. H., 2008, *arXiv: 0811.1218*
- Stewart K. R., Bullock J. S., Wechsler R. H., Maller A. H., Zentner A. R., 2008, *ApJ*, 683, 597
- Tacconi L. J., et al., 2008, *ApJ*, 680, 246
- Taylor J. E., Babul A., 2005, *MNRAS*, 364, 535
- Tegmark M., et al., 2006, *Phys. Rev. D*, 74, 123507
- Thacker R. J., Scannapieco E., Couchman H. M. P., 2006, *ApJ*, 653, 86
- Toomre A., Toomre J., 1972, *ApJ*, 178, 623
- Tormen G., 1998, *MNRAS*, 297, 648
- Tormen G., Moscardini L., Yoshida N., 2004, *MNRAS*, 350, 1397
- Vale A., Ostriker J. P., 2006, *MNRAS*, 371, 1173
- van den Bosch F. C., Tormen G., Giocoli C., 2005, *MNRAS*, 359, 1029
- Wang L., Kauffmann G., 2008, *MNRAS*, 391, 785
- Wang L., Li C., Kauffmann G., De Lucia G., 2006, *MNRAS*, 371, 537
- Wetzel A. R., Cohn J. D., White M., 2009, *MNRAS*, p. in press
- Wetzel A. R., Schulz A. E., Holz D. E., Warren M. S., 2008, *ApJ*, 683, 1
- White M., 2001, *A&A*, 367, 27
- White M., 2002, *ApJS*, 143, 241
- White S. D. M., Rees M. J., 1978, *MNRAS*, 183, 341
- Yamauchi C., Yagi M., Goto T., 2008, *MNRAS*, 390, 383
- Yang X., Mo H. J., van den Bosch F. C., 2009, *ApJ*, 693, 830
- Yoshida M., et al., 2006, *ApJ*, 653, 988
- Zentner A. R., Berlind A. A., Bullock J. S., Kravtsov A. V., Wechsler R. H., 2005, *ApJ*, 624, 505
- Zhang J., Ma C.-P., Fakhouri O., 2008, *MNRAS*, 387, L13